Oxidative Addition of the Fluoromethane C−F Bond to Pd. An ab Initio Benchmark and DFT Validation Study

G. Theodoor de Jong and F. Matthias Bickelhaupt*

Afdeling Theoretische Chemie, Scheikundig Laboratorium der Vrije Universiteit, De Boelelaan 1083, NL-1081 HV Amsterdam, The Netherlands

Received: June 30, 2005; In Final Form: August 26, 2005

We have computed a state-of-the-art benchmark potential energy surface (PES) for two reaction pathways (oxidative insertion, OxIn, and S_N2) for oxidative addition of the fluoromethane C−F bond to the palladium atom and have used this to evaluate the performance of 26 popular density functionals, covering LDA, GGA, meta-GGA, and hybrid density functionals, for describing these reactions. The ab initio benchmark is obtained by exploring the PES using a hierarchical series of ab initio methods (HF, MP2, CCSD, CCSD(T)) in combination with a hierarchical series of seven Gaussian-type basis sets, up to *g* polarization. Relativistic effects are taken into account through a full four-component all-electron approach. Our best estimate of kinetic and thermodynamic parameters is −5.3 (−6.1) kcal/mol for the formation of the reactant complex, 27.8 (25.4) kcal/mol for the activation energy for oxidative insertion (OxIn) relative to the separate reactants, 37.5 (31.8) kcal/mol for the activation energy for the alternative S_N2 pathway, and −6.4 (−7.8) kcal/mol for the reaction energy (zero-point vibrational energy-corrected values in parentheses). Our work highlights the importance of sufficient higher angular momentum polarization functions for correctly describing metal-*d*-electron correlation. Best overall agreement with our ab initio benchmark is obtained by functionals from all three categories, GGA, meta-GGA, and hybrid DFT, with mean absolute errors of 1.4−2.7 kcal/mol and errors in activation energies ranging from 0.3 to 2.8 kcal/mol. The B3LYP functional compares very well with a slight underestimation of the overall barrier for OxIn by −0.9 kcal/mol. For comparison, the well-known BLYP functional underestimates the overall barrier by −10.1 kcal/mol. The relative performance of these two functionals is inverted with respect to previous findings for the insertion of Pd into the C−H and C−C bonds. However, all major functionals yield correct trends and qualitative features of the PES, in particular, a clear preference for the OxIn over the alternative S_N2 pathway.

1. Introduction

The activation of the C−F bond in fluorocarbons provides a great challenge for synthetic chemists. Fluorocarbons are known to have a high chemical inertness and high thermal stability. This is caused by the great strength of the C−F bond. Fluorine is the most electronegative element and forms the strongest single bond with carbon of any element.[1] Examples of carbon−fluorine bond activation by metal complexes have been given but are relatively rare.[2,3] Catalytic activation of the C−F bond can provide means to selectively convert simple fragments into desired complex products via C−C bond formation. Successful examples have been found for, inter alia, aryl fluorides.[4] While C−H and C−C bond activation has been the subject in various computational investigations, the oxidative addition of the C−F or, more generally, the C-halogen bonds has received much less attention.[5] Still, there is a few number of computational studies[5−14] on the activation of C−X bonds by d^{10} metal centers, such as palladium complexes, which is one of our main subjects of interest because of its relevance for homogeneous catalysis.[15]

Transition-metal-induced C−F bond activation usually proceeds via an oxidative addition process in which the metal increases its formal oxidation state by two units. There has been controversy about the mechanism of this reaction.[2] One mechanism that has been proposed requires the concerted transfer of two electrons and involves either a concerted front-side displacement or a concerted nucleophilic displacement (S_N2) proceeding via backside attack of the C−F bond by the metal. Theoretical studies on the oxidative addition of the C−Cl bond of chloromethane to the Pd atom show[6,13] that this process can indeed proceed via direct oxidative insertion of the metal into the C−Cl bond (OxIn) or via S_N2 substitution followed, in a concerted manner, by leaving-group rearrangement (S_N2-ra). The reaction barrier for OxIn is lower than that for the S_N2 pathway. Interestingly, anion assistance, e.g., coordination of a chloride anion to Pd, reverses this order in activation energies and makes S_N2 the preferred pathway. Note that this shift in mechanism also corresponds to a change in stereochemistry at the carbon atom involved, namely, from retention (OxIn) to inversion of configuration (S_N2). This is of practical relevance for substrates in which the carbon atom, C*, is asymmetric (which is obviously not the case in the simple model of chloromethane). Now, one may wonder if these two pathways, schematically represented in Chart 1, exist also for the corresponding activation of the stronger and more polar C−F bond.

Besides answering the above question, the present study aims at two objectives. In the first place, we wish to obtain a reliable benchmark for the potential energy surface (PES) for the oxidative addition of the C−F bond of fluoromethane to Pd(0). This is done by exploring this PES with a hierarchical series of

* Corresponding author fax: +31-20-59 87629; e-mail: fm.bickelhaupt@few.vu.nl.

10.1021/jp053587i CCC: $30.25
Published on Web 10/05/2005

CHART 1: Model Reaction and Nomenclature

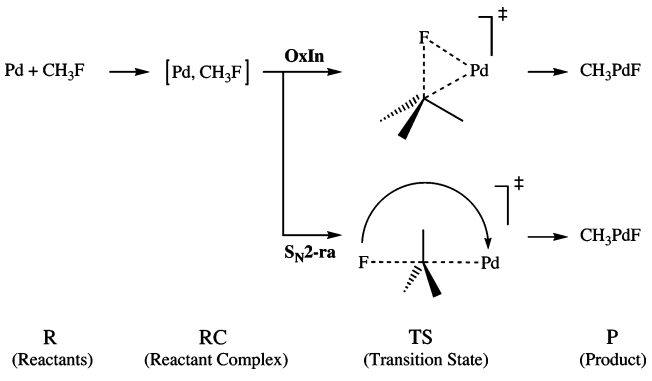

ab initio methods [Hartree−Fock (HF), second-order Møller−Plesset perturbation theory (MP2),[16] and coupled cluster theory[17] with single and double excitations (CCSD),[18] and with triple excitations treated perturbatively (CCSD(T))[19]] in combination with a hierarchical series of Gaussian-type basis sets of increasing flexibility and polarization (up to *g* functions). The basis set superposition error (BSSE) is accounted for by counterpoise correction (CPC).[20] Relativistic effects are treated with a full four-component all-electron approach. To our knowledge these are the first benchmarking calculations at advanced correlated levels for this model reaction.

Recently, with the same approach, we have investigated the insertion of the Pd-d^{10} atom into the C−H bond of methane and the C−C bond of ethane as important examples of oxidative addition reactions to Pd.[21−23] Density functional theory[24−26] (DFT) was shown to reproduce the highest-level ab initio (coupled-cluster) benchmark potential energy surfaces (PESs) within a few kcal/mol.[22,23] Interestingly, the well-known BLYP functional turned out to be among the best performing functionals, providing PESs that are better than those of most of the high-level meta-GGA and hybrid functionals. The present model reaction of Pd + CH_3F may possibly impose higher demands to the basis set used in the computations than the previously studied model reactions of Pd + CH_4 or C_2H_6 because the fluorine atom expands relatively much when it gains anionic character (which is what happens in an oxidative addition). Therefore, we have also investigated the oxidative addition of hydrogen fluoride to Pd. This model system is computationally less demanding than Pd + CH_3F and thus allows to extend the basis set further, in fact, just far enough, in our attempt to test for convergence of the CCSD(T) energies with basis-set size.

The second purpose of our work is to evaluate the performance of 26 popular density functionals, covering LDA, GGA, meta-GGA, and hybrid density functionals, for describing the oxidative addition of the fluoromethane C−F bond to Pd, using the ab initio benchmark as reference point. Here, we anticipate that while the latter turns out to be satisfactory in terms of accuracy and reliability, it is prohibitively expensive if one wishes to study more realistic model catalysts and substrates. Thus, our survey of 26 density functionals serves to validate one or more of these DFT approaches as a computationally more efficient alternative to high-level ab initio theory in future investigations in the field of computational catalysis.[14] A general concern, however, associated with the application of DFT to the investigation of chemical reactions is its notorious tendency to underestimate activation energies.[9,27−32] Furthermore, we investigate the dependence of the resulting PES on the basis-set size and on the use of the frozen-core approximation. Thus, we arrive at a ranking of density functional approaches in terms of the accuracy with which they describe the PES of our model reaction, in particular the activation energy. We focus on the overall activation energy, that is, the difference in energy between the transition state and the separate reactants, which is decisive for the rate of chemical reactions in the gas phase, in particular, if they occur under low-pressure conditions in which the reaction system is (in good approximation) thermally isolated[33,34] (see also section II of ref 35). But we also address the central barrier, that is, the difference in energy between the transition state and the reactant complex.

2. Method and Computational Details

2.1. Geometries. All geometry optimizations have been done with DFT using the Amsterdam Density Functional (ADF) program.[36−39] For functionals, both LDA and GGA, the performance for computing the geometries and relative energies of the stationary points along the PES of our model reaction (see Chart 1) was compared. These density functionals are the LDA functional VWN[40] and the GGA functionals BP86,[41,42] BLYP,[41,43] PW91,[44−47] PBE,[48,49] revPBE,[50] RPBE,[51] and OLYP.[43,52] They were used in combination with the TZ2P basis set, which is a large uncontracted set of Slater-type orbitals (STOs) containing diffuse functions, which is of triple-ζ quality and has been augmented with two sets of polarization functions: 2*p* and 3*d* on H, 3*d* and 4*f* on C and F, and 5*p* and 4*f* on Pd. The core shells of carbon and fluorine (1*s*) and palladium (1*s*2*s*2*p*3*s*3*p*3*d*) were treated by the frozen-core approximation.[36] An auxiliary set of *s*, *p*, *d*, *f*, and *g* STOs was used to fit the molecular density and to represent the Coulomb and exchange potentials accurately in each SCF cycle.[36] Relativistic effects were accounted for using the zeroth-order regular approximation (ZORA).[53] For each of the eight functionals, all stationary points were confirmed to be equilibrium structures (no imaginary frequencies) or a transition state (one imaginary frequency) through vibrational analysis. Enthalpies at 298.15 K and 1 atm were calculated from 0 K electronic energies according to the following equation, assuming an ideal gas (eq 1):

$$\Delta H_{298} = \Delta E + \Delta E_{\mathrm{trans},298} + \Delta E_{\mathrm{rot},298} + \Delta E_{\mathrm{vib},0} + \Delta(\Delta E_{\mathrm{vib},0})_{298} + \Delta(pV) \quad (1)$$

Here, $\Delta E_{\mathrm{trans},298}$, $\Delta E_{\mathrm{rot},298}$, and $\Delta E_{\mathrm{vib},0}$ are the differences between products and reactants in translational, rotational, and zero-point vibrational energy, respectively; $\Delta(\Delta E_{\mathrm{vib},0})_{298}$ is the change in the vibrational energy difference going from 0 to 298.15 K. The vibrational energy corrections are based on our frequency calculations. The molar work term $\Delta(pV)$ is $(\Delta n)RT$; $\Delta n = -1$ for two reactants (Pd + CH_3F) combining to one species. Thermal corrections for the electronic energy are neglected.

2.2. Ab Initio Calculations. Based on the ZORA-BLYP/TZ2P geometries, energies of the stationary points were computed in a series of single-point calculations with the program package DIRAC[54,55] using the following hierarchy of quantum chemical methods: HF, MP2, CCSD, and CCSD(T). Relativistic effects are accounted for using a full all-electron four-component Dirac-Coulomb approach with a spin-free Hamiltonian (SFDC).[56] The two-electron integrals over exclusively the small components have been neglected and corrected with a simple Coulombic correction, which has been shown reliable.[57]

A hierarchical series of Gaussian-type basis sets was used (see Table 1). For carbon, hydrogen, and fluorine Dunning's correlation consistent augmented double-ζ (cc-aug-pVDZ), triple-ζ (cc-aug-pVTZ), quadruple-ζ (cc-aug-pVQZ), and quin-

TABLE 1: Basis Sets Used in the ab Initio Calculations

name	Pd	C	H	F
BS1	(24*s*16*p*13*d*)[a]	cc-aug-pVDZ[b]	cc-aug-pVDZ[b]	cc-aug-pVDZ[b]
BS2	(24*s*16*p*13*d*)[a] + 1*f*	cc-aug-pVDZ[b]	cc-aug-pVDZ[b]	cc-aug-pVDZ[b]
BS3	(24*s*16*p*13*d*)[a] + 4*f*	cc-aug-pVDZ[b]	cc-aug-pVDZ[b]	cc-aug-pVDZ[b]
BS4	(24*s*16*p*13*d*)[a] + 4*f* + *p*	cc-aug-pVDZ[b]	cc-aug-pVDZ[b]	cc-aug-pVDZ[b]
BS5	(24*s*16*p*13*d*)[a] + 4*f* + *p* + *g*	cc-aug-pVDZ[b]	cc-aug-pVDZ[b]	cc-aug-pVDZ[b]
BS6	(24*s*16*p*13*d*)[a] + 4*f* + *p* + *g*	cc-aug-pVDZ[b]	cc-aug-pVDZ[b]	cc-aug-pVTZ[b]
BS6*	(24*s*16*p*13*d*)[a] + 4*f* + *p* + *g*		cc-aug-pVTZ[b]	cc-aug-pVTZ[b]
BS7	(24*s*16*p*13*d*)[a] + 4*f* + *p* + *g*	cc-aug-pVDZ[b]	cc-aug-pVDZ[b]	cc-aug-pVQZ[b]
BS8	(24*s*16*p*13*d*)[a] + 4*f* + *p* + *g*		cc-aug-pVDZ[b]	cc-aug-pV5Z[b]

[a] TZP quality. [b] Completely uncontracted.

tuple-ζ (cc-aug-pV5Z) basis sets were used.[58,59] These were used in uncontracted form because it is technically difficult to use contracted basis sets in the kinetic balance procedure in DIRAC.[60] The basis set of palladium is based on an uncontracted basis set (24*s*16*p*13*d*), which is of triple-ζ quality, and has been developed by K. Faegri, Jr. (personal communication). The combination of this basis set for palladium and the aforementioned cc-aug-pVDZ basis sets for carbon, hydrogen, and fluorine is denoted BS1 (see Table 1). As a first extension, in BS2, one set of 4*f* polarization functions was added with an exponent of 1.472, as reported by Ehlers et al.[61] In BS3, this single set of 4*f* functions was substituted by four sets of 4*f* polarization functions as reported by Langhoff and co-workers with exponents 3.611217, 1.29541, 0.55471, and 0.23753.[62] Thereafter, going to BS4, an additional set of diffuse *p* functions was introduced with exponent 0.141196, as proposed by Osanai et al.[63] BS5 was created by adding a set of *g* functions, with an exponent of 1.031690071. This value is close to but not exactly equal to the exponent of the *g* functions optimized by Osanai. Instead it is equal to the value of one of the exponents of the *d* set of Faegri, which reduces computational costs.

Note that the basis sets BS1−BS5 used in the present study (see Table 1) correspond in quality to the basis sets BS1−BS5 used in our recent study on the oxidative insertion of Pd into the C−C bond of ethane (see Table 2 in ref 23). For the latter model reaction, relative energies were converged to within ca. 1 kcal/mol at BS5. In the present study, we wish to further extend the series of basis sets regarding their flexibility because of the possibly increased demands, in this respect, of fluorine (see also the Introduction). For our model system CH_3F + Pd, it was possible to go until BS6 and BS7, which are extensions of BS5, replacing the basis set for fluorine with uncontracted cc-aug-pVTZ and uncontracted cc-aug-pVQZ, respectively (see Table 1). Larger basis sets appeared to be unfeasible as this would cause the required memory to exceed our available allotment. Thus, to yet further extend our exploration of basis-set convergence, in terms of computational costs (in particular memory) a less demanding model reaction system Pd + HF was included into this investigation. This model reaction was also studied with basis sets BS5, BS6, and BS7, but furthermore with BS6*, which is an extension of BS6, replacing the basis set for hydrogen with uncontracted cc-aug-pVTZ, and with BS8, in which an uncontracted cc-aug-pV5Z basis set is used for fluorine (for a schematic overview, see Table 1).

2.3. DFT Calculations. Based on the ZORA-BLYP/TZ2P geometries, we have also evaluated, in a series of single-point calculations, how the ZORA-BLYP relative energies of stationary points along the PES depend on the basis-set size for four different all-electron (i.e., no frozen-core approximation) STO basis sets, namely ae-DZ, ae-TZP, ae-TZ2P, and ae-QZ4P, and on the use of the frozen-core approximation. The ae-DZ basis set is of double-ζ quality, is unpolarized for C, F, and H, but has been augmented with a set of 5*p* polarization functions for Pd. The ae-TZP basis set is of triple-ζ quality and has been augmented with one set of polarization functions on every atom: 2*p* on H, 3*d* on C and F, and 5*p* on Pd. The ae-TZ2P basis set (the all-electron counterpart corresponding to the above-mentioned TZ2P basis that is used in conjunction with the frozen-core approximation) is also of triple-ζ quality and has been augmented with two sets of polarization functions on each atom: 2*p* and 3*d* on H, 3*d* and 4*f* on C and F, and 5*p* and 4*f* on Pd. The ae-QZ4P basis set is of quadruple-ζ quality and has been augmented with four sets of polarization functions on each atom: two 2*p* and two 3*d* sets on H, two 3*d* and two 4*f* sets on C and F, and two 5*p* and two 4*f* sets on Pd.

Finally, based again on the ZORA-BLYP/TZ2P geometries, we have computed in a post-SCF manner, i.e., using in all cases the electron density obtained at ZORA-BLYP/ae-TZ2P, the relative energies of stationary points along the PES for various LDA, GGAs, meta-GGAs, and hybrid functionals. In addition to the ones used in the geometry optimizations (see section 2.1), the following density functionals were examined: the GGA-functionals Becke 88x + BR89c,[64,65] FT97,[66] HCTH/93,[67] BOP,[64,68] HCTH/120,[69] HCTH/147,[69] and HCTH/407;[70] the meta-GGA functionals BLAP3,[71] VS98,[72] KCIS,[73] PKZB,[74,75] Bmτ1,[76] OLAP3,[52,71] and TPSS;[77,78] and the hybrid functionals B3LYP,[79,80] O3LYP,[81] X3LYP[82] (all based on VWN5[83]), and TPSSh.[77,78]

3. Results and Discussion

3.1. Geometries of Stationary Points and Characteristics of the Addition Reaction. First, we examine the geometries of stationary points along the reaction coordinates of the two pathways for oxidative addition of the C−F bond of fluoromethane to Pd, computed with the LDA functional VWN and the GGA functionals BP86, BLYP, PW91, PBE, revPBE, RPBE, and OLYP in combination with the TZ2P basis set, the frozen-core approximation, and the zeroth-order regular approximation (ZORA) to account for relativistic effects. Geometry parameters for selected stationary points are defined in Figure 1, and their values optimized with each of the eight functionals are collected in Table 2.

For each of the functionals the reaction characteristics are similar. For both reaction pathways, OxIn and S_N2-ra, the reaction proceeds from the reactants R via formation of a stable reactant complex RC of C_s symmetry, in which fluoromethane coordinates via two hydrogen atoms in an η^2 fashion to Pd (see Figure 1), completely analogous to the corresponding reactant complexes of Pd + methane[22] and Pd + ethane.[23] In the OxIn pathway, the reaction proceeds from this RC via a transition state TS_{OxIn} of C_s symmetry to the final product P of C_s symmetry. The alternative S_N2-ra pathway brings the system from the same reactant complex RC in three different steps,

TABLE 2: Selected Geometry Parameters[a] (in Å, deg), Optimized with Eight Different Density Functionals and the TZ2P Basis Set with Frozen-Core Approximation,[b] of Selected Stationary Points along the Reaction Coordinates of the OxIn and S_N2-Type Pathways for Oxidative Addition of the C−F Bond of CH_3F to Pd

method		C−F	C−H(1)	C−H(2)	Pd−C	Pd−F	Pd−H(1)	∠(F−C−H(1))	∠(C−Pd−F)
VWN	R	1.374	1.102					109.3	
	RC	1.373	1.161	1.100	2.125		1.846	108.9	
	TS_{OxIn}	1.756	1.201	1.094	1.970	2.173	1.834	136.6	49.9
	$TS_{S_N2\text{-ra}}$	2.573	1.542	1.107	1.934	2.433	2.062	8.3	71.1
	P[c]	2.756	1.104	1.099	1.936	1.882	2.462	121.1	92.4
BP86	R	1.400	1.098					108.7	
	RC	1.399	1.137	1.096	2.273		1.943	108.4	
	TS_{OxIn}	1.783	1.182	1.090	2.045	2.266	1.869	136.6	48.5
	$TS_{S_N2\text{-ra}}$	2.569	1.513	1.104	1.991	2.498	2.117	7.9	68.8
	P	2.894	1.104	1.095	1.978	1.923	2.465	143.9	95.8
BLYP	R	1.413	1.095					108.4	
	RC	1.411	1.123	1.094	2.390		2.031	108.2	
	TS_{OxIn}	1.785	1.158	1.086	2.129	2.297	1.907	134.3	47.4
	$TS_{S_N2\text{-ra}}$	2.569	1.501	1.101	2.025	2.526	2.148	7.9	67.7
	P	2.949	1.102	1.093	2.004	1.944	2.483	143.1	96.7
PW91	R	1.398	1.096					108.8	
	RC	1.397	1.135	1.095	2.271		1.942	108.4	
	TS_{OxIn}	1.779	1.180	1.088	2.042	2.267	1.867	136.9	48.4
	$TS_{S_N2\text{-ra}}$	2.568	1.514	1.102	1.987	2.506	2.111	7.7	68.6
	P[c]	2.857	1.098	1.093	1.977	1.926	2.496	121.1	94.1
PBE	R	1.398	1.098					108.8	
	RC	1.397	1.138	1.096	2.268		1.941	108.4	
	TS_{OxIn}	1.779	1.183	1.090	2.039	2.266	1.867	137.1	48.5
	$TS_{S_N2\text{-ra}}$	2.569	1.512	1.104	1.987	2.513	2.121	7.7	68.5
	P	2.886	1.104	1.096	1.974	1.925	2.464	144.2	95.5
revPBE	R	1.405	1.099					108.7	
	RC	1.404	1.132	1.097	2.338		1.990	108.4	
	TS_{OxIn}	1.792	1.179	1.090	2.060	2.296	1.882	137.3	48.2
	$TS_{S_N2\text{-ra}}$	2.567	1.492	1.106	2.003	2.544	2.139	7.5	67.6
	P	2.921	1.105	1.096	1.986	1.940	2.475	144.0	96.2
RPBE	R	1.407	1.099					108.7	
	RC	1.406	1.130	1.097	2.361		2.008	108.3	
	TS_{OxIn}	1.794	1.178	1.090	2.067	2.307	1.886	137.4	48.0
	$TS_{S_N2\text{-ra}}$	2.568	1.495	1.106	2.007	2.553	2.146	7.5	67.3
	P	2.931	1.105	1.097	1.989	1.945	2.477	143.9	96.4
OLYP	R	1.395	1.095					108.8	
	RC[d]	1.389	1.128	1.094	3.088		1.966	108.8	
	TS_{OxIn}	1.798	1.165	1.086	2.055	2.295	1.899	138.4	48.4
	$TS_{S_N2\text{-ra}}$	2.546	1.472	1.102	1.993	2.569	2.147	7.2	66.4
	P	2.938	1.101	1.092	1.970	1.944	2.455	143.4	97.3

[a] See Figure 1 for definition. [b] Relativistic effects treated with ZORA (see section 2.1). [c] Pd−F bond orientated eclipsed with respect to the C−H(2) bond, at variance with the product geometries for the other functionals; see text. [d] CH_3F coordinated to Pd in $\eta1$ instead of $\eta2$ fashion, i.e., via one instead of two hydrogen atoms, namely H(1); see text.

i.e., in a more complex manner than suggested in Chart 1, to the same product P (see Figure 1). Interestingly, the minimal energy path of the Pd atom approach to the C atom in a backside fashion first leads to insertion into a C−H bond. The transition state for insertion of Pd into the fluoromethane C−H bond, TS_{CH} (3.0 kcal/mol above reactants, computed at BLYP), is very similar to the corresponding transition state for Pd + methane (3.9 kcal/mol above reactants),[22] but the resulting product of this insertion, i.e., intermediate IM_{CH} (at −7.1 kcal/mol) is somewhat more stabilized with respect to the reactants than the corresponding species for methane (at −3.4 kcal/mol).[22] Thereafter, in step 2, the inserted Pd does not approach much further; however, the F− leaving group is expelled from carbon and in a concerted movement, via transition state TS_{S_N2} (26.4 kcal/mol), it abstracts the young hydrogen ligand, as a proton, from Pd. The product of this second elementary step, intermediate IM_{S_N2} (12.1 kcal/mol relative to reactants), can be conceived as a complex between the relatively stable $PdCH_2$ entity and HF (this complex is bound by −6.6 kcal/mol, again at BLYP). In intermediate IM_{S_N2}, the CH_2-end can rotate almost freely, with a rotation barrier of 0.9 kcal/mol. Because of the presence of this intermediate, there will be racemization, which is a notable difference with the OxIn pathway in which there is retention of configuration. This difference will, of course, only be noticed for chiral substrates and not for our simple, achiral fluoromethane model substrate. Finally, the third and last elementary step proceeds from intermediate IM_{S_N2} via transition state $TS_{S_N2\text{-ra}}$ to the same final product P as for the OxIn pathway. Transition state $TS_{S_N2\text{-ra}}$ is 30.2 kcal/mol (again at BLYP) above the reactants and, thus, constitutes the highest point on the PES along the S_N2-ra pathway. As this will be the rate-determining point, at least for the gas-phase process occurring in the low-pressure regime, and for economic reasons, we confine our determination of a high-level ab initio benchmark PES for the S_N2-ra pathway to the stationary points R, RC, $TS_{S_N2\text{-ra}}$, and P.

We wish to point out the two marked differences between the S_N2-ra mechanism of the present Pd + CH_3F system and that of Pd + CH_3Cl, studied previously.[6,13,14] In both cases, there are two competing reaction channels, direct oxidative insertion (OxIn) and an alternative pathway with strong S_N2 character (S_N2-ra). In the first place, however, the C−F bond is much stronger than the C−Cl bond, and activation of the former is associated with significantly higher barriers (via both OxIn and S_N2). Thus, at variance with the situation for Pd + CH_3Cl,[16] the minimum energy path for Pd approaching CH_3F from the

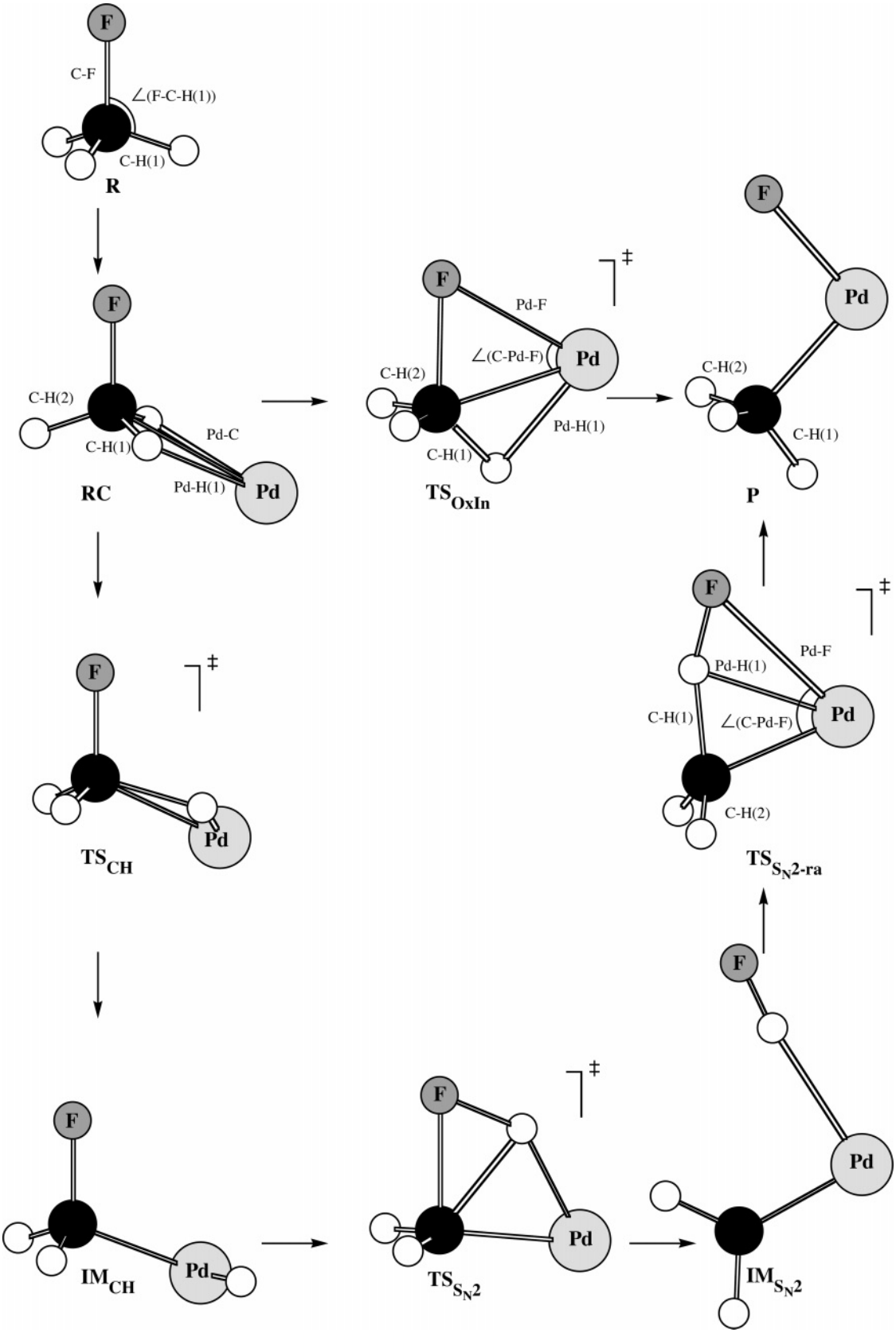

Figure 1. Structures of stationary points along the reaction coordinates of the OxIn and S_N2-type pathways for the oxidative addition of the fluoromethane C−F bond to Pd. See Table 2 for values of geometry parameters for selected stationary points.

backside is, in a sense, redirected from straight nucleophilic substitution and proceeds instead via the relatively low-energy saddle point TS_{CH} for insertion into a C−H bond. Furthermore, for both, Pd + CH_3F and Pd + CH_3Cl, the highest point on the PES of the S_N2-ra pathway has the character of a migrating leaving group, i.e., F- and Cl-, respectively. However, the much higher basicity of F- compared to Cl- causes the former, after its expulsion in TS_{S_N2} and on its way toward Pd, to abstract a proton, under formation of the intermediate IM_{S_N2}. At variance, in the case of Pd + CH_3Cl,[16] the expelled Cl- leaving group

migrates directly to Pd *without abstracting a proton* and, thus, without forming an additional intermediate complex involving the conjugate acid HCl.

All species in both reaction pathways have been verified through vibrational analyses to represent equilibrium structures (no imaginary frequencies) or transition states (one imaginary frequency). Furthermore, it has been verified that each transition state connects the stable stationary points as reported. The imaginary frequency in transition state TS_{OxIn} associated with the normal mode that connects reactant complex and product varies for the GGA functionals between 453 and 471 i cm^{-1} (for BP86, BLYP, PW91, PBE, revPBE, RPBE, and OLYP it amounts to 471, 454, 463, 466, 456, 453, and 453 i cm^{-1}); for the LDA functional VWN, this imaginary frequency is somewhat larger and amounts to 501 i cm^{-1}. The imaginary frequency in transition state $TS_{S_N2\text{-}ra}$ associated with the normal mode that connects intermediate IM_{S_N2} and product varies for the GGA functionals between 835 and 1005 i cm^{-1} (for BP86, BLYP, PW91, PBE, revPBE, RPBE, and OLYP it amounts to 867, 1005, 835, 842, 932, 952, and 961 i cm^{-1}); for the LDA functional VWN, this imaginary frequency is somewhat smaller and amounts to 683 i cm^{-1}.

The geometries obtained with the various LDA and GGA functionals do not show significant mutual discrepancies (see Table 2 and Figure 1). The two most eye-catching, but not essential, differences are the reactant complex RC computed with OLYP and the product P computed with VWN and PW91. Contrary to the situation found previously for methane[22] and ethane[23] substrates, OLYP yields an η^1 instead of an η^2 reactant complex. It should be noted, however, that forcing Pd in RC into an η^2 geometry will raise the energy with only a mere 0.6 kcal/mol. Likewise, VWN and PW91 yield a product in which the methyl group is in an eclipsed instead of a staggered conformation relative to the Pd−F bond but, again, this difference is not exactly dramatic if one realizes that the eclipsed is higher in energy than the staggered conformer by only 0.2 kcal/mol for VWN and a virtually negligible 0.03 kcal/mol for PW91. In fact, the essential physics here is that the methyl group is virtually a free internal rotor.

The C−H bond distance values are very robust with respect to changing the functional, with variations in the order of a few hundredths, or less, of an Å. Note that variations in the length of the activated C−F bond become larger as the reaction progresses, in the product up to 0.09 Å along the various GGA functionals. This is in line with the fact that this bond is being broken along the reaction coordinate, which causes the PES to become increasingly soft in this coordinate and, thus, sensitive to changes in the computational method. More pronounced variations are found for the weak Pd−C and Pd−H bonds. This holds especially for the loosely bound reactant complex, which for the GGA functionals show fluctuations of up to one tenth of an Å for Pd−C and in the order of some hundredths up to one tenth for Pd−H (LDA deviates a bit more, up to a few tenths of an Å). The variations in these bond distances drop to a few hundredths or even a few thousandths of an Å as the reaction proceeds to the product in which more stable coordination bonds are formed. Thus, only moderate (although not negligible) variations in bond distances occur along the various functionals, and they are more pronounced for the softer (or broken) bonds. This is, of course, also reflected by the variations in bond angles. These variations are very small as firmly bound triplets of atoms are involved but can become somewhat larger for angles opposite to a soft bond.

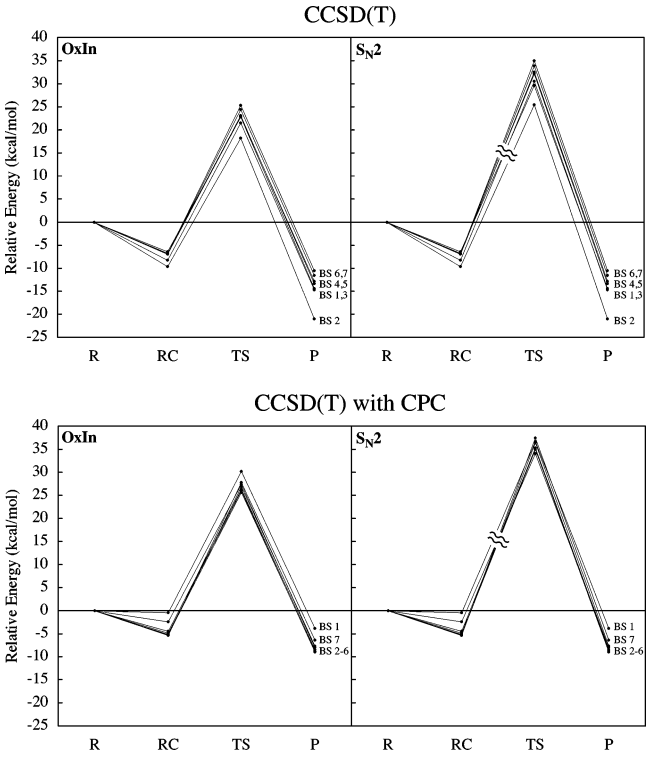

Figure 2. Reaction profiles for the OxIn and S_N2-type pathways for the oxidative addition of the fluoromethane C−F bond to Pd, computed with CCSD(T) for various basis sets, without (upper panel) and with counterpoise correction (lower panel). Geometries optimized at ZORA-BLYP/TZ2P, i.e., with frozen-core approximation.

Thus, the various functionals yield essentially the same geometries. Since we found in previous studies on the reaction of Pd with methane and ethane that BLYP performs excellently in terms of relative energies of stationary points for those model reactions[22,23] and because BLYP is robust and well established, we choose the geometries of this functional, i.e., ZORA-BLYP/TZ2P, to compute the ab initio benchmark potential energy surface in the next section.

3.2. Benchmark Energies from Ab Initio Calculations. Here, we report the first systematic ab initio calculations into relative energies of the model addition reaction of the C−F bond of fluoromethane to the Pd atom. This survey is based on geometries of stationary points that were optimized at the ZORA-BLYP/TZ2P level of relativistic DFT (see the preceding section and Table 2). The results of our ab initio computations are collected in Tables 3 and 4 (relative energies and BSSE) and graphically displayed in Figure 2 (reaction profiles). Table S1 in the Supporting Information shows the total energies in a.u. of all species occurring at the stationary points as well as the total energies of the corresponding Pd and fluoromethane fragments, with and without the presence of the other fragment as ghost. In this way, we can calculate the BSSE and carry out a counterpoise correction (CPC).

We proceed with examining the reaction profiles of the two pathways for oxidative addition of the fluoromethane C−F bond to Pd, that is, the energies of the stationary points relative to the reactants Pd and fluoromethane, which are collected in Table 3 and, for CCSD(T), displayed in Figure 2. At all levels of theory except Hartree−Fock, the reaction profiles are characterized by the formation of a stable reactant complex (RC), which leads via the transition state for direct oxidative insertion (TS_{OxIn}) or via the transition state for rearrangement after an S_N2-type reaction ($TS_{S_N2\text{-}ra}$) to the oxidative addition product (P). Three striking observations can be made: (i) the spread in values of

TABLE 3: Relative Energies (in kcal/mol) of Selected Stationary Points of Interest along the Reaction Coordinates of the Two Pathways for Oxidative Addition of Pd to the C−F Bond of CH_3F, without (no CPC) and with Counterpoise Correction (with CPC), Computed at Several Levels of ab Initio Theory

		RC		TS_{OxIn}		$TS_{S_N2\text{-}ra}$		P	
method	basis set	no CPC	with CPC	no CPC	with CPC	no CPC	with CPC	no CPC	with CPC
HF	BS1	9.9	10.5	60.7	61.3	71.9	72.5	26.3	27.0
	BS2	9.8	10.4	60.1	60.8	70.9	71.5	23.4	24.1
	BS3	9.5	10.2	59.4	60.2	69.7	70.4	20.5	21.4
	BS4	9.4	10.1	59.4	60.1	69.6	70.3	20.3	21.2
	BS5	9.4	10.0	59.2	59.9	69.3	70.0	19.6	20.4
	BS6	9.5	10.0	60.9	61.5	70.4	71.0	21.0	21.7
	BS7	9.5	10.0	61.4	61.9	70.8	71.3	21.5	22.1
MP2	BS1	−5.1	−0.4	24.0	29.9	34.5	40.2	−8.4	0.5
	BS2	−9.7	−3.0	17.3	25.9	28.4	36.5	−16.4	−3.6
	BS3	−9.1	−5.9	19.1	23.2	32.9	36.9	−7.3	−1.9
	BS4	−8.0	−6.2	20.2	23.0	34.0	36.6	−6.5	−2.3
	BS5	−8.5	−6.8	19.5	22.2	33.8	36.4	−5.9	−2.0
	BS6	−8.5	−6.9	20.7	23.2	35.1	37.5	−4.9	−1.5
	BS7	−8.5	−7.0	21.4	23.9	36.0	38.4	−4.1	−0.6
CCSD	BS1	−3.8	1.0	30.2	36.2	37.0	42.7	−8.9	−0.1
	BS2	−6.4	−0.4	26.9	34.5	34.5	41.7	−14.0	−2.9
	BS3	−4.8	−2.1	30.0	33.6	39.3	42.8	−7.9	−3.2
	BS4	−4.1	−2.4	30.8	33.3	40.1	42.6	−7.5	−3.7
	BS5	−4.2	−2.6	30.7	33.1	40.5	42.9	−6.8	−3.3
	BS6	−4.1	−2.7	32.4	34.6	42.0	44.2	−5.3	−2.2
	BS7	−4.1	−2.8	33.4	35.6	43.1	45.3	−4.2	−1.0
CCSD(T)	BS1	−6.3	−0.4	22.8	30.2	29.6	36.7	−14.4	−3.9
	BS2	−9.6	−2.4	18.3	27.4	25.4	34.0	−21.0	−8.0
	BS3	−8.2	−4.4	21.5	26.3	30.5	35.3	−14.7	−8.5
	BS4	−6.7	−4.8	23.1	26.0	32.1	35.0	−13.3	−8.9
	BS5	−6.9	−5.1	22.9	25.7	32.5	35.2	−12.8	−8.8
	BS6	−6.8	−5.3	24.4	26.9	33.9	36.4	−11.5	−7.7
	BS7	−6.8	−5.3	25.3	27.8	35.0	37.5	−10.5	−6.4

TABLE 4: Basis Set Superposition Error (BSSE, in kcal/mol) for Pd and CH_3F in Selected Stationary Points of Interest along the Reaction Coordinates of the Two Pathways for Oxidative Addition of Pd to the C−F Bond of CH_3F, Computed at Several Levels of ab Initio Theory

		RC			TS_{OxIn}			$TS_{S_N2\text{-}ra}$			P		
method	basis set	Pd	CH_3F	total	Pd	CH_3F	total	Pd	CH_3F	total	Pd	CH_3F	total
HF	BS1	0.5	0.2	0.6	0.5	0.1	0.6	0.5	0.1	0.6	0.5	0.2	0.7
	BS2	0.5	0.2	0.6	0.5	0.2	0.6	0.5	0.1	0.6	0.5	0.2	0.7
	BS3	0.5	0.2	0.7	0.5	0.3	0.7	0.5	0.2	0.7	0.5	0.4	0.9
	BS4	0.4	0.3	0.7	0.4	0.3	0.7	0.4	0.3	0.7	0.4	0.4	0.8
	BS5	0.4	0.3	0.7	0.4	0.3	0.7	0.4	0.3	0.7	0.4	0.4	0.9
	BS6	0.4	0.1	0.5	0.4	0.2	0.6	0.4	0.2	0.6	0.4	0.2	0.7
	BS7	0.4	0.1	0.5	0.4	0.2	0.6	0.4	0.1	0.6	0.4	0.2	0.6
MP2	BS1	4.3	0.4	4.7	5.3	0.6	5.9	5.1	0.6	5.7	7.8	1.1	8.9
	BS2	6.3	0.4	6.7	8.0	0.6	8.6	7.5	0.6	8.1	11.7	1.1	12.8
	BS3	2.5	0.6	3.1	3.0	1.1	4.0	2.9	1.1	4.0	3.5	1.9	5.4
	BS4	1.1	0.7	1.8	1.4	1.3	2.7	1.4	1.3	2.7	2.1	2.1	4.2
	BS5	1.0	0.7	1.8	1.3	1.3	2.7	1.3	1.3	2.6	1.7	2.2	3.9
	BS6	1.1	0.5	1.6	1.5	0.9	2.4	1.4	1.1	2.4	2.1	1.3	3.4
	BS7	1.1	0.4	1.5	1.7	0.8	2.4	1.5	1.0	2.4	2.5	1.0	3.5
CCSD	BS1	4.4	0.4	4.8	5.4	0.6	6.0	5.1	0.6	5.7	7.8	1.0	8.8
	BS2	5.6	0.4	5.9	7.0	0.6	7.6	6.6	0.6	7.2	10.0	1.0	11.1
	BS3	2.1	0.6	2.7	2.5	1.0	3.5	2.5	1.0	3.5	3.0	1.7	4.7
	BS4	1.0	0.7	1.7	1.3	1.2	2.5	1.2	1.3	2.5	1.9	1.9	3.8
	BS5	0.9	0.7	1.6	1.2	1.3	2.4	1.1	1.3	2.4	1.5	2.0	3.5
	BS6	0.9	0.5	1.4	1.3	0.9	2.2	1.2	1.0	2.2	1.8	1.3	3.0
	BS7	0.9	0.4	1.3	1.4	0.7	2.2	1.3	0.9	2.2	2.2	1.0	3.2
CCSD(T)	BS1	5.5	0.4	5.9	6.7	0.6	7.4	6.4	0.7	7.0	9.4	1.1	10.5
	BS2	6.8	0.4	7.2	8.4	0.6	9.1	8.0	0.7	8.6	11.8	1.2	13.0
	BS3	3.2	0.6	3.8	3.7	1.1	4.8	3.6	1.2	4.8	4.3	1.9	6.2
	BS4	1.1	0.8	1.9	1.5	1.4	2.9	1.4	1.4	2.9	2.2	2.2	4.4
	BS5	1.0	0.8	1.8	1.3	1.4	2.7	1.3	1.5	2.7	1.7	2.3	4.0
	BS6	1.1	0.5	1.6	1.5	1.0	2.5	1.4	1.1	2.5	2.1	1.8	3.9
	BS7	1.1	0.4	1.5	1.7	0.8	2.5	1.5	1.0	2.5	2.5	1.6	4.1

computed relative energies, depending on the level of theory and basis set, is enormous, up to nearly 45 kcal/mol; (ii) the size of the BSSE is also remarkably large, up to ca. 13 kcal/mol; and (iii) convergence with basis-set size of the computed energies is still not reached with standard basis sets used routinely in CCSD(T) computations on organometallic and coordination compounds. The lack of any correlation leads to a complete failure at the HF level, which yields an unbound RC and strongly exaggerated activation barriers: ca. 62 kcal/mol for TS_{OxIn} and ca. 71 kcal/mol for $TS_{S_N2\text{-}ra}$. The failure of

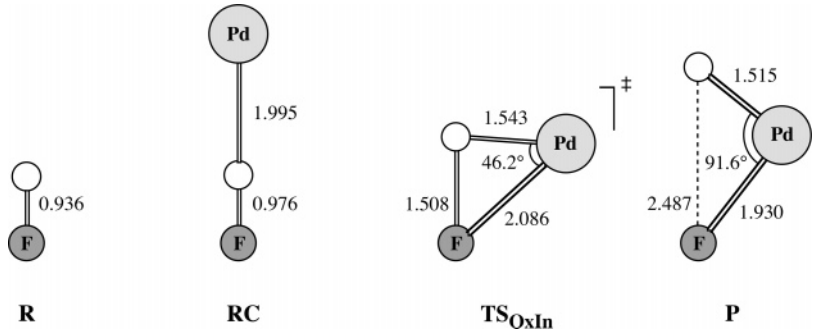

Figure 3. Structures of stationary points along the reaction coordinate for the oxidative addition of H−F to Pd. Geometries optimized at ZORA-BLYP/TZ2P, i.e., with frozen-core approximation.

HF for describing the PES of our model reaction is not unexpected because electron correlation, which is not contained in this approach, is important.[84,85] The activation energies for both pathways drop significantly when electron correlation is introduced. Along HF, CCSD, and CCSD(T) in combination with basis set BS1, for example, the activation barrier for direct oxidative insertion decreases from 60.7 to 30.2 to 22.8 kcal/mol. But also the correlated CCSD(T) values obtained with basis sets BS1 up to BS3, comparable in quality to standard basis sets such as LANL2DZ[86,87] without or with up to four *f* functions added, are questionable, as they are obviously not converged as a function of the basis-set size. For example, at CCSD(T)/BS1 the activation energy for direct insertion is 22.8 kcal/mol. This activation energy computed at CCSD(T) drops from 22.8 kcal/mol for basis set BS1 to 18.3 kcal/mol for basis set BS2 in which one *f* polarization function has been added. Thereafter, along BS2 to BS5, the activation energy increases again, although not monotonically, from 21.5 to 22.9 kcal/mol, as three more sets of *f* functions, an additional set of diffuse *p* functions, and a set of *g* functions are added to the basis set of Pd. When the basis set for fluorine is also increased, to uncontracted cc-aug-pVTZ (BS6) and uncontracted cc-aug-pVQZ (BS7), the activation energy further increases from 24.4 to 25.3 kcal/mol, respectively (see Tables 1 and 3). This is illustrated by Figure 2, upper diagrams, which shows the CCSD(T) reaction profiles for the two reaction pathways and how they vary along basis sets BS1−BS7.

Next, we note that the BSSE takes on large values in the correlated ab initio methods, whereas it is negligible if correlation is completely neglected, i.e., in HF (see Table 4). The BSSE increases somewhat going from BS1 to BS2, decreases from BS2 to BS5, and remains more or less constant from BS5 to BS7. At the CCSD(T) level, for example, the BSSE for TS_{OxIn} amounts to 7.4, 9.1, 4.8, 2.9, 2.7, 2.5, and 2.5 kcal/mol along the basis sets BS1−BS7, whereas the corresponding BSSE values at HF are only ca. 0.7 kcal/mol (Table 4). The BSSE increases along the reaction coordinate, i.e., going from RC to TS_{OxIn} to P or going from RC to $TS_{SN2\text{-}ra}$ to P. The reason for this is that along these series of stationary points, the carbon, hydrogen, and fluorine atoms and, thus, their basis functions come closer too and begin to surround the palladium atom. This effectively improves the flexibility and polarization of the basis set and thus the description of the wave function in the region of the palladium atom. Note that, for basis sets BS1−BS3, the BSSE stems predominantly from the improvement of the stabilization of palladium as fluoromethane ghost functions are added. This contribution to the BSSE quickly reduces as the basis set of palladium is improved; for BS4 and BS5 (which contain *g* as well as diffuse *p* functions on Pd), it has become approximately equal to or slightly smaller than the extra stabilization of the fluoromethane fragment due to adding palladium ghost functions. Further increasing the basis set on fluorine, going to BS6 and BS7, leads again to a slightly larger contribution from the extra stabilization of the palladium fragment and a slightly smaller one from the fluoromethane fragment. The total BSSE remains more or less constant. Note that the total BSSE at CCSD(T) has been considerably decreased, i.e., for TS_{OxIn}, from 9.1 kcal/mol for BS2 to only 2.5 kcal/mol for BS7 (Table 4) and is thus clearly smaller than the relative energies that we wish to be able to compute accurately, in particular activation energies, such as that for direct insertion, which amounts to 25.3 kcal/mol; see CCSD(T)/BS7 in Table 3.

The high sensitivity of the PES for oxidative addition of the fluoromethane C−F bond to Pd highlights the prominent role that electron correlation plays in our model systems. It is striking that the relative CCSD(T) energies have still not reached convergence for basis set BS3, which is of a quality comparable to that of standard basis sets such as LANL2DZ,[86] augmented with four *f* polarization functions, for Pd (see Table 3 and Figure 2, upper; see also above). This may be somewhat surprising in view of earlier reports that such basis sets yield satisfactory energies for organometallic and coordination compounds (see, for example, the excellent reviews by Frenking et al.[84] and by Cundari et al.[85]). On the other hand, it is consistent with our findings for the PESs for oxidative addition of the methane C−H bond and the ethane C−C bond to Pd, which show the same sensitivity and behavior.[21,23] One reason for the increased sensitivity that we find toward the quality of the theoretical approach is that the presence of *f* polarization functions is only the minimum requirement for describing the electron correlation of palladium 4*d* electrons. In this respect, the palladium basis sets in BS1, BS2, and BS3 should be considered minimal and cannot be expected to have achieved convergence. Furthermore, the consequences of any inadequacy in the basis set shows up more severely in processes such as ours, which involve a bare, uncoordinated transition-metal atom as one of the reactants because here the effect of additional assistance of basis functions on the substrate is more severe than in situations where the transition-metal fragment is already surrounded, e.g., by ligands, before it combines with the substrate. This shows up in the relatively large BSSE values for CCSD(T)/BS1−BS3.

To ensure that convergence is reached for the basis-set size of the substrate atoms, particularly the fluorine atom, we have extended our investigations to the oxidative insertion of Pd into the H−F bond of hydrogen fluoride. This model reaction, in which fluorine also occurs in a polar bond, is computationally less demanding and therefore enables us to use larger basis sets than would be possible for our main model system CH_3F. Geometries of stationary points were obtained at the ZORA-BLYP/TZ2P level and are given in Figure 3. The insertion of Pd into the H−F bond has a significant barrier and is slightly

TABLE 5: Relative Energies (in kcal/mol) of the Stationary Points along the Reaction Coordinate for Oxidative Addition of Pd to the H−F Bond of HF, without (no CPC) and with Counterpoise Correction (with CPC), Computed at Several Levels of ab Initio Theory

		RC		TS_{OxIn}		P	
method	basis set	no CPC	with CPC	no CPC	with CPC	no CPC	with CPC
HF	BS5	3.3	3.5	52.9	53.6	31.1	31.9
	BS6	3.4	3.5	54.3	54.8	32.2	32.7
	BS6*	3.4	3.4	54.5	55.0	32.5	33.0
	BS7	3.4	3.5	54.5	54.9	32.4	32.8
	BS8	3.5	3.6	54.6	55.1	32.6	33.0
MP2	BS5	−2.2	−1.5	20.4	22.9	19.0	22.3
	BS6	−2.1	−1.7	20.0	22.1	18.4	21.1
	BS6*	−2.9	−0.9	18.5	21.1	16.8	20.0
	BS7	−2.2	−1.7	19.5	21.7	17.9	20.7
	BS8	−2.2	−0.6	19.1	22.6	17.4	20.7
CCSD	BS5	−1.5	−0.8	25.4	27.5	10.9	13.5
	BS6	−1.3	−1.0	25.8	27.6	11.0	13.2
	BS6*	−2.0	−0.4	24.7	27.0	9.9	12.6
	BS7	−1.3	−1.0	25.8	27.6	10.8	13.1
	BS8	−1.4	−0.1	25.3	28.3	10.3	13.2
CCSD(T)	BS5	−2.5	−1.7	19.2	21.8	6.7	9.6
	BS6	−2.4	−1.9	19.3	21.4	6.4	8.9
	BS6*	−3.3	−1.3	18.0	20.6	5.2	8.2
	BS7	−2.4	−2.0	19.1	21.2	6.1	8.8
	BS8	−2.5	−1.1	18.7	21.9	5.6	8.8

endothermic (complexation, activation, and reaction energy at BLYP, respectively, −5.0, 12.1, and 0.5 kcal/mol). The results of the ab initio calculations for Pd + HF with basis sets BS5, BS6, BS6* (new), BS7, and BS8 (new) are collected in Table 5 (see Table S2 in the Supporting Information for the corresponding total energies). Note that along BS5−BS8, the basis set for Pd is the same and corresponds to the largest one used for Pd + CH_3F. Only the basis sets for H and F are varied (see also Table 1).

The PES for Pd + HF shows similar trends along HF, MP2, CCSD, and CCSD(T) as Pd + CH_3F. The lack of any correlation at Hartree−Fock leads again to a highly exaggerated activation barrier and an unbound reactant complex (see Table 5). Furthermore, relative energies are reasonably, i.e., within ca. 1 kcal/mol, converged at all basis sets used for fluorine and hydrogen, i.e., BS5−BS8. For example, the activation energy (i.e., TS_{OxIn} relative to R) for Pd + HF at CCSD(T) with counterpoise correction varies from 21.8, 21.4, 20.6, 21.2, to 21.9 along the basis sets BS5, BS6, BS6*, BS7, and BS8 (see Table 5). The variations found for the complexation (i.e., RC relative to R) and reaction energy (i.e., P relative to R) are not larger. We conclude that, for the oxidative insertion of Pd into a polar bond involving fluorine, the relative energies calculated with a basis set at triple- or quadruple-ζ level for fluorine are reliable to within a kcal/mol. This further corroborates the benchmark calculations for the oxidative addition reactions of Pd + CH_3F.

Thus, we have been able to achieve virtual convergence of the CCSD(T) relative energies by using a larger than standard basis set and by correcting for the BSSE through counterpoise correction; see Table 3 and Figure 2, lower. Indeed, along BS2−BS7, for TS_{OxIn}, the BSSE decreases monotonically from 9.1 to 4.8 to 2.9 to 2.7 to 2.5 to 2.5 kcal/mol and is thus clearly smaller than the relative energies that we compute (see Tables 3 and 4). This legitimates the use of counterpoise correction (CPC) as a means to correct for the BSSE. The counterpoise-corrected relative energies at CCSD(T) are converged to ca. 1 kcal/mol. For example, the counterpoise-corrected activation energy for direct oxidative insertion (OxIn) at CCSD(T) amounts to 30.2, 27.4, 26.3, 26.0, 25.7, 26.9, and 27.8 kcal/mol (Table 3). Our best estimate, obtained at CCSD(T)/BS7 with CPC, for the kinetic and thermodynamic parameters of the oxidative insertion of Pd into the fluoromethane C−F bond is −5.3 kcal/mol for the formation of the reactant complex, 27.8 kcal/mol for the activation energy (relative to reactants) of the direct oxidative insertion pathway, 37.5 kcal/mol for the activation energy (relative to reactants) of the S_N2 pathway for oxidative addition, and −6.4 kcal/mol for the reaction energy (see Table 6). If we take into account zero-point vibrational energy (ZPE) effects computed at BLYP/TZ2P, this yields −6.1 kcal/mol for the formation of the reactant complex, 25.4 kcal/mol for the activation energy for the direct insertion pathway, 31.8 kcal/mol for the activation energy for the S_N2 pathway, and −7.8 kcal/mol for the reaction energy (see Table 6).

3.3. Validation of DFT. Next, we examine the relative energies of stationary points computed with the LDA functional VWN and the GGA functionals BP86, BLYP, PW91, PBE, revPBE, RPBE, and OLYP in combination with the TZ2P basis set, the frozen-core approximation, and the zeroth-order regular approximation (ZORA) to account for relativistic effects. Note that for each density functional we use consistently the geometries optimized with that functional, for example, BP86//BP86 or BLYP//BLYP (see section 3.1). As pointed out in the Introduction, we first focus on the overall activation energy, that is, the difference in energy between the transition state and

TABLE 6: Relative Energies without (ΔE) and with Zero-Point Vibrational Energy Correction ($\Delta E + \Delta ZPE$), and Relative Enthalpies at 298.15 K (ΔH) of Selected Stationary Points of Interest[a] along the Reaction Coordinates of the Two Pathways for Oxidative Addition of Pd to the C−F Bond of CH_3F (in kcal/mol), Computed with Eight Different Density Functionals and the TZ2P Basis Set with Frozen-Core Approximation,[b] and Compared to the ab Initio Benchmark from This Work

	ΔE				$\Delta E + \Delta ZPE$				ΔH			
method	RC	TS_{OxIn}	$TS_{S_N2\text{-}ra}$	P	RC	TS_{OxIn}	$TS_{S_N2\text{-}ra}$	P	RC	TS_{OxIn}	$TS_{S_N2\text{-}ra}$	P
DFT Computations (This Work)[b]												
VWN	−26.1	−0.8	15.3	−30.8	−27.2	−3.2	10.2	−32.2	−27.8	−4.0	9.7	−32.5
BP86	−9.7	14.0	27.3	−18.3	−10.6	11.5	21.8	−19.8	−11.0	10.8	21.3	−20.0
BLYP	−5.5	17.7	30.2	−15.8	−6.2	15.3	24.5	−17.2	−6.4	14.7	24.1	−17.4
PW91	−11.3	12.4	26.0	−19.6	−12.0	10.0	20.5	−21.0	−12.5	9.3	20.1	−21.2
PBE	−10.8	12.8	26.4	−18.9	−11.7	10.3	20.9	−20.5	−12.1	9.7	20.4	−21.2
revPBE	−5.4	18.3	30.9	−14.1	−6.2	15.9	25.3	−15.6	−6.5	15.2	24.9	−15.8
RPBE	−4.9	18.8	31.3	−13.6	−5.7	16.3	25.6	−15.1	−6.0	15.7	25.2	−15.2
OLYP	−1.1	25.3	37.6	−6.2	−1.4	22.9	31.9	−7.7	−1.6	22.2	31.5	−7.9
Ab Initio Benchmark (This Work)[c]												
CCSD(T) // BLYP	−5.3	27.8	37.5	−6.4	−6.1	25.4	31.8	−7.8				

[a] Geometries and energies computed at the same level of theory. See Figure 1 for structures. [b] Relativistic effects treated with ZORA (see section 2.1). [c] CCSD(T) benchmark from this work.

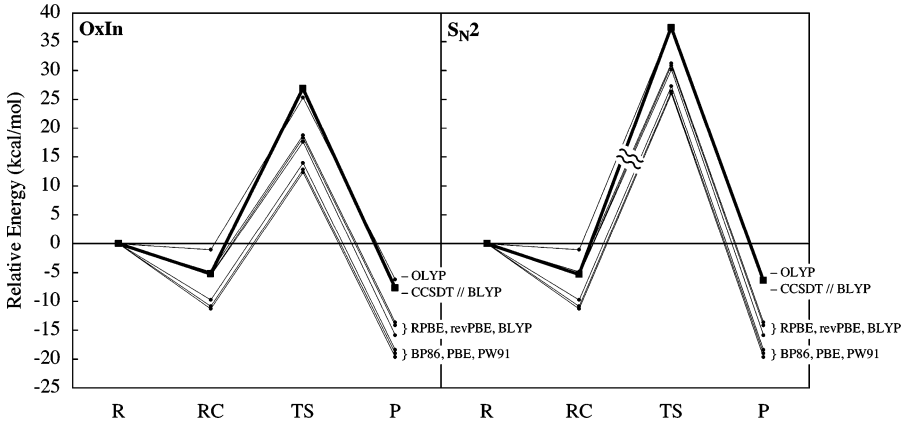

Figure 4. Reaction profiles for the OxIn and S_N2-type pathways for the oxidative addition of the fluoromethane C−F bond to Pd, obtained with seven different GGA density functionals (thin lines) and the TZ2P basis set, i.e., with frozen-core approximation (geometries and energies computed at the same level of DFT; relativistic effects are treated with ZORA). The counterpoise-corrected CCSD(T) benchmark of this work is also included (thick lines).

the separate reactants, which is decisive for the rate of chemical reactions in the gas phase, in particular, if they occur under low-pressure conditions. Later on, in section 3.4, we also address the central barrier, that is, the difference in energy between the transition state and the reactant complex. Relative energies, with and without zero-point vibrational energy correction, as well as relative enthalpies are collected in Table 6. Relative energies for the GGA functionals are also graphically represented in Figure 4. The performance of the LDA functional VWN and the seven different GGA functionals is assessed by a systematic comparison of the resulting potential energy surfaces with our relativistic four-component CCSD(T) benchmark. It is clear from Table 6 that LDA suffers here from its infamous overbinding providing barriers that are too low and complexation and reaction energies that are too high. The GGA functionals, as can be seen in Figure 4, fall into three groups regarding their agreement with the benchmark results. OLYP is clearly the best performing functional, with barriers for both reaction pathways and a reaction energy that agree within ca. 2 kcal/mol with the CCSD(T) benchmark. The other functionals overestimate metal−substrate bonding in the reactant complex and provide a too low barrier and a too exothermic reaction energy. The apparent overbinding is more pronounced for BP86, PBE, and PW91 than for BLYP, revPBE, and RPBE. For example, PW91 underestimates the barrier for direct insertion by 15.4 kcal/mol and the barrier for the alternative S_N2-ra pathway by 11.5 kcal/mol, whereas BLYP underestimates these barriers by 10.1 and 7.3 kcal/mol. Note however that all seven GGA functionals yield the same relative order in barriers and reaction energies, that is, OxIn well beneath S_N2, in nice agreement with the CCSD(T) benchmark. This parallels our previous findings for the oxidative addition of the methane C−H and ethane C−C bond to Pd.[22,23] However, in the latter model reactions, i.e., C−H and C−C activation, BLYP agrees excellently with CCSD(T) and OLYP *overestimates* barriers by 5−7 kcal/mol, at variance with the present case of C−F activation for which it is OLYP that agrees excellently with CCSD(T) and BLYP that *underestimates* barriers by 7−10 kcal/mol.

We proceed with examining the convergence of the (all-electron) BLYP relative energies of stationary points as the basis set increases along ae-DZ, ae-TZP, ae-TZ2P, and ae-QZ4P, using the ZORA-BLYP/TZ2P geometries, which were also used in the ab initio calculations in the preceding section (see Table 2). We also investigate the convergence of the BSSE along this series of basis sets as well as the effect of using the frozen-core approximation in the calculations discussed in the preceding paragraph. The results are shown in Table 7 and in Figure 5. In the first place, we note that it is valid to use the frozen-core approximation as it has only small effects on the relative energies. This becomes clear if one compares the relative energies obtained with frozen-core BLYP/TZ2P in Table 6 (−5.5, 17.7, 30.2, and −15.8 kcal/mol for RC, TS_{OxIn}, $TS_{S_N2\text{-ra}}$, and P) with the corresponding all-electron BLYP/ae-TZ2P data in Table 7 (no CPC: −5.4, 17.7, 30.2, and −16.3 kcal/mol for RC, TS_{OxIn}, $TS_{S_N2\text{-ra}}$, and P). The frozen-core and all-electron values of the relative energies agree for the RC, TS_{OxIn}, and $TS_{S_N2\text{-ra}}$ within 0.1 kcal/mol and only for the product they differ more, namely 0.5 kcal/mol. Next, the issue of basis set convergence is addressed. The data in Table 7 show that, except for the products, the relative energies of stationary points are already converged to within the order of half a kcal/mol with the ae-TZ2P basis set. The BSSE drops to 0.6 kcal/mol or less for this basis set and becomes even smaller, i.e., less than 0.3 kcal/mol, if one goes to ae-QZ4P (see Table 7: the BSSE is the difference between "no CPC" and "with CPC" values). For example, the activation energy for the OxIn pathway, without counter-poise correction varies from 14.0 to 18.0 to 17.7 to 17.3 kcal/mol along ae-DZ, ae-TZP, ae-TZ2P, and ae-QZ4P (Table 7, no CPC). The corresponding BSSE amounts to 3.9, 0.3, 0.3, and 0.1 kcal/mol (see Table 7). Note that in fact the BSSE is large, i.e., a few kcal/mol, only for the smallest, ae-DZ, basis set. This is in line with our previous work on the oxidative addition of methane and ethane to Pd in which we found that basis-set convergence and elimination of the BSSE are achieved much earlier for DFT (e.g., BLYP or B3LYP) than

TABLE 7: Relative Energies (in kcal/mol) of Selected Stationary Points of Interest[a] along the Reaction Coordinates of the Two Pathways for Oxidative Addition of Pd to the C−F Bond of CH_3F, Computed with BLYP and Four Different Basis Sets with All Electrons Treated Variationally, without (no CPC) and with Counterpoise Correction (with CPC)[b]

	RC		TS_{OxIn}		$TS_{S_N2\text{-ra}}$		P	
basis set	no CPC	with CPC	no CPC	with CPC	no CPC	with CPC	no CPC	with CPC
ae-DZ	−1.3	1.0	14.0	17.9	28.9	32.6	−18.2	−14.4
ae-TZP	−4.9	−4.6	18.0	18.3	30.9	31.3	−14.2	−13.6
ae-TZ2P	−5.4	−5.1	17.7	18.0	30.2	30.6	−16.3	−15.7
ae-QZ4P	−5.6	−5.5	17.3	17.4	29.8	29.9	−16.5	−16.2

[a] Geometries optimized at ZORA-BLYP/TZ2P with frozen-core approximation, see Figure 1. [b] Relativistic effects treated with ZORA (see section 2.1).

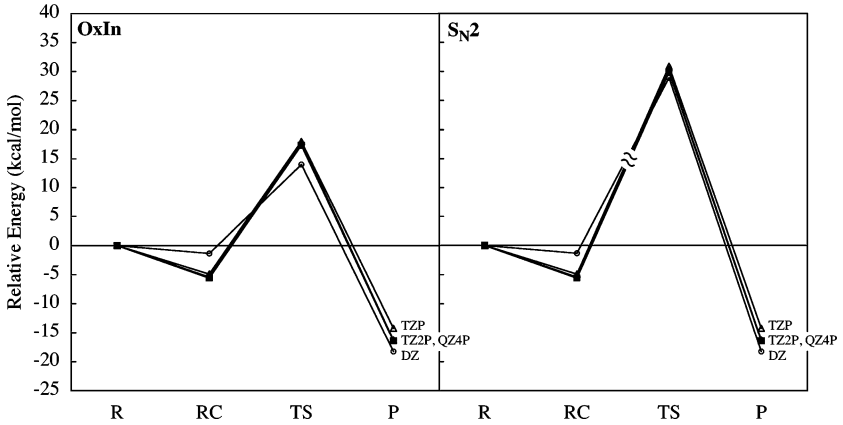

Figure 5. Reaction profiles for the OxIn and S_N2-type pathways for the oxidative addition of the fluoromethane C−F bond to Pd, computed with ZORA-BLYP and four different basis sets with all electrons treated variationally, without counterpoise correction. Geometries optimized at ZORA-BLYP/TZ2P, i.e., using the frozen-core approximation.

for correlated ab initio methods, e.g., CCSD(T).[21−23] In general, correlated ab initio methods depend more strongly on the extent of polarization of the basis set because the polarization functions are essential to generate the configurations through which the wave function can describe the correlation hole. In DFT, on the other hand, the correlation hole is built-in into the potential, and the energy functional and polarization functions mainly play the much less delicate role of describing polarization of the electron density. In conclusion, the TZ2P basis in combination with the frozen-core approximation yields an efficient and accurate (i.e., within a kcal/mol) description of the relative energies of our stationary points.

Finally, based again on the ZORA-BLYP/TZ2P geometries discussed above, we have computed the relative energies of stationary points along the PES for various LDA, GGAs, meta-GGAs, and hybrid functionals in combination with the all-electron ae-TZ2P basis set and ZORA for relativistic effects. This was done in a post-SCF manner, i.e., using density functionals with the electron density obtained at ZORA-BLYP/ae-TZ2P. The performance of the density functionals is discussed by comparing the resulting potential energy surfaces with that of the ab initio (CCSD(T)) benchmark discussed above. The results of this survey are collected in Table 8, which shows energies relative to the separate reactants (R). Energies relative to the reactant complex are summarized in Table 9 and will be discussed in section 3.4.

For clarity, we wish to point out that the above procedure for computing the relative energies shown in Table 8 differs in three respects from that used for computing the relative energies with the LDA functional and the seven GGA functionals shown in Table 6: (i) an all-electron approach is used instead of the frozen-core approximation, (ii) for all density functionals, the BLYP optimized geometries are used instead of geometries optimized with the same functional, and (iii) for all functionals, the BLYP electron density is used for computing the energy instead of the electron density corresponding to that functional. The effect of going from frozen-core (TZ2P) to all-electron calculations (ae-TZ2P), i.e., point (i), is small, causing a stabilization of 0.5 kcal/mol or less, and has already been discussed above. The differences between the values in Tables 6 and 8 derive mainly from the combined effect of points (ii) and (iii), which in the case of the GGA functionals causes a destabilization of up to 1.4 kcal/mol (for the OLYP reactant complex) of the relative energies if one goes from Table 6 to Table 8. Both effects are in the order of a few tenths of a kcal/mol up to maximally one kcal/mol and, for the different GGA functionals and stationary points, contribute to this destabilization with varying relative importance. For example, for TS_{OxIn}, the single-point approach contributes generally somewhat more (0.3−0.6 kcal/mol) to this destabilization than the post-SCF approach (0.1−0.4 kcal/mol). This has been assessed by computing the relative energies of stationary points using approximation (ii) but not (iii), i.e., computing them with the electron density corresponding to the density functional under consideration but with the BLYP geometries; the resulting values are provided in parentheses in Table 8. In conclusion, for the GGA functionals, the combined effect of approximations (i)−(iii) on the relative energies of stationary points is in the order of a kcal/mol with an upper limit of 1.4 kcal/mol.

Now, we extend our survey to the full range of energy density functionals that, except for LDA and the seven GGAs discussed above, have been implemented in the ADF program in a post-SCF manner. For all 26 density functionals, we have computed the mean absolute error in the relative energies of reactant complex, transition states and product, and the error in the barriers, i.e., the relative energy of the transition states, as compared with the CCSD(T) benchmark (see Table 8). Both the mean absolute error and the error in the barrier drop significantly if one goes from LDA (mean abs. err. = 21.4 kcal/mol), which as mentioned above suffers from its infamous overbinding, to GGA functionals (mean abs. err. = 2.1−11.1 kcal/mol). However, no significant improvement occurs if one goes from GGA to the more recently developed meta-GGA functionals (mean abs. err. = 2.7−10.0 kcal/mol). Going to the more sophisticated hybrid functionals again gives improvement (mean abs. err. = 1.4−5.6 kcal/mol). Best overall agreement with the ab initio benchmark PES is achieved by functionals of the GGA (HCTH/407 and OLYP) and meta-GGA (BLAP3 and Bmτ1) as well as hybrid-DFT type (B3LYP and X3LYP), with mean absolute errors of 1.4 to 2.2 kcal/mol and errors in the barriers ranging from −2.1 to −0.9 kcal/mol for the direct insertion pathway and from 0.3 to 2.8 kcal/mol for the alternative S_N2-ra pathway. Note that the outstanding performance of BLYP with respect to other functionals (e.g., OLYP and B3LYP), found for insertion of Pd into C−H and C−C bonds, does not hold for insertion of Pd into C−F bond. Here, BLYP has a mean absolute error of 6.9 kcal/mol which has to be compared with 2.2 kcal/mol for OLYP and even 1.5 kcal/mol for B3LYP. In particular, BLYP underestimates the barrier for OxIn by −10.1 kcal/mol and the barrier for S_N2-ra by −7.4 kcal/mol. Again, note that OLYP and B3LYP perform much better for these barriers: both slightly underestimate the barrier for OxIn (by −1.8 and −0.9 kcal/mol, respectively) and both slightly

TABLE 8: Energies (kcal/mol) Relative to the Separate Reactants (R) of Selected Stationary Points of Interest[a] along the Reaction Coordinates of the Two Pathways for Oxidative Addition of Pd to the C−F Bond of CH_3F, and Dissociation Energy of CH_3F into a Methyl Radical and Fluorine Atom (D_{CF}), Computed for 26 Different Density Functionals with the ae-TZ2P Basis Set with All Electrons Treated Variationally[b]

method	RC		TS_{OxIn}		$TS_{S_N2\text{-ra}}$		P		mean abs. err. rel. to R[c]	err. in OxIn barr. rel. to R[c]	err. in S_N2-ra barr. rel. to R[c]	D_{CF}	err. in D_{CF}[d]
						LDA							
VWN	−21.4	(−21.7)	2.3	(2.0)	16.6	(16.7)	−29.4	(−29.5)	21.4	−25.4	−20.9	142.2	30.3
						GGAs							
BP86	−9.0	(−9.1)	14.6	(14.5)	27.5	(27.5)	−18.6	(−18.6)	9.8	−13.2	−10.0	116.6	4.7
BLYP	−5.4		17.7		30.1		−16.3		6.9	−10.1	−7.4	114.6	2.7
Becke88x + BR89c	−6.1		17.4		29.6		−18.7		7.8	−10.4	−7.8	115.5	3.6
PW91	−10.5	(−10.5)	13.1	(13.0)	26.1	(26.2)	−19.7	(−19.8)	11.1	−14.7	−11.4	119.3	7.5
PBE	−10.0	(−10.1)	13.7	(13.4)	26.6	(26.6)	−19.0	(−19.2)	10.6	−14.0	−10.9	118.8	6.9
FT97	−10.8		15.5		26.6		−17.6		9.9	−12.2	−10.8	111.7	−0.2
revPBE	−5.0	(−5.1)	19.0	(18.7)	31.1	(31.0)	−14.3	(−14.5)	5.9	−8.8	−6.4	112.1	0.2
HCTH/93	0.1		26.6		39.4		−5.1		2.5	−1.2	2.0	114.7	2.8
RPBE	−4.5	(−4.7)	19.4	(19.1)	31.5	(31.4)	−13.8	(−14.0)	5.6	−8.4	−6.0	111.2	−0.7
BOP	−2.1		21.5		33.3		−13.0		5.1	−6.2	−4.2	113.2	1.3
HCTH/120	−4.2		21.6		35.1		−9.6		3.2	−6.2	−2.4	117.0	5.1
HCTH/147	−3.5		22.2		35.8		−9.2		3.0	−5.5	−1.7	116.9	5.1
HCTH/407	−1.6		25.6		38.8		−5.1		2.1	−2.1	1.4	115.7	3.8
OLYP	0.3	(−0.2)	26.0	(25.6)	38.5	(37.9)	−6.2	(−6.5)	2.2	−1.8	1.0	113.7	1.9
						Meta-GGAs							
BLAP3	0.4		26.6		37.8		−10.1		2.7	−1.1	0.3	116.9	5.0
VS98	−9.3		12.2		29.0		−18.6		10.0	−15.6	−8.5	111.7	−0.1
KCIS	−7.0		15.0		29.0		−18.4		8.8	−12.8	−8.5	111.6	−0.3
PKZB	−5.5		16.4		30.9		−17.8		7.4	−11.4	−6.6	109.2	−2.6
Bmτ1	0.7		26.9		37.9		−10.0		2.7	−0.9	0.5	115.2	3.4
OLAP3	6.2		34.9		46.2		−0.1		8.4	7.1	8.7	116.1	4.2
TPSS	−7.0		15.9		31.5		−18.6		7.9	−11.8	−6.0	113.5	1.6
						Hybrid Functionals							
B3LYP	−3.4		26.9		40.2		−7.0		1.5	−0.9	2.7	110.9	−1.0
O3LYP	0.3		31.0		45.2		−0.4		5.6	3.3	7.7	116.1	4.3
X3LYP	−3.9		26.8		40.3		−6.9		1.4	−1.0	2.8	111.2	−0.6
TPSSh	−5.7		20.8		36.4		−13.6		3.9	−7.0	−1.0	111.0	−0.8

[a] Geometries optimized at ZORA-BLYP/TZ2P with frozen-core approximation, see Figure 1. [b] Computed post-SCF using the BLYP electron density, unless stated otherwise. Values in parentheses computed self-consistently, i.e., with the potential and electron-density corresponding to the energy functional indicated. Relativistic effects treated with ZORA (see section 2.1). [c] Mean absolute error for the energies of the four stationary points RC, TS_{OxIn}, $TS_{S_N2\text{-ra}}$, and P relative to the separate reactants (R) and error in the overall barriers, i.e., in the energy of the TS_{OxIn}, respectively $TS_{S_N2\text{-ra}}$, relative to R, compared with the CCSD(T) benchmark from this work. [d] Error in the dissociation energy of the C−F bond in fluoromethane, compared with CCSD(T) benchmark from this work, which amounts to 111.9 kcal/mol (see section 3.4).

overestimate the barrier for S_N2-ra (by 1.0 and 2.7 kcal/mol, respectively).

3.4. Performance for the Central Barrier. So far, we have concentrated on the overall activation energy, that is, the difference in energy between the TS and separate reactants which, as pointed out earlier, is decisive for the rate of chemical reactions in the gas phase, in particular, if they occur under low-pressure conditions in which the reaction system is (in good approximation) thermally isolated.[33−35] Here, we address the central barrier, that is, the difference in energy between the transition state and the reactant complex. The latter becomes decisive in the high-pressure regime, when termolecular collisions are sufficiently efficient to cool the otherwise rovibrationally hot reactant complex, causing it to be in thermal equilibrium with the environment. It may be tempting to conceive the central barrier of the gas-phase reaction as the barrier of the same process in solution. We stress, however, that this is not in general the case, because differential solvation of the reactant complex and the transition state can affect the barrier height substantially, even to the extent that relative heights of barriers for competing processes can be inverted (see, for example, refs 88 and 89, and references therein). In Table 9, we have collected the energies of the separate reactants (R), the transition states of both reaction pathways (TS_{OxIn} and $TS_{S_N2\text{-ra}}$), and the product (P) relative to the reactant complex (RC).

The mean absolute error changes by changing the point of reference from the separate reactants (in Table 8) to the reactant complex (in Table 9). Best overall performance is again achieved by the hybrid functionals X3LYP (mean abs. err. = 1.8 kcal/mol) and B3LYP (mean abs. err. = 2.0 kcal/mol). They outperform BLYP (mean abs. err. = 6.8 kcal/mol) and also OLYP (mean abs. err. = 5.8 kcal/mol). Here, B3LYP appears to perform remarkably well for both, energies relative to reactants (R) and relative to the reactant complex (RC).

We have verified to which extent errors made, e.g., by BLYP or B3LYP in overall or central barriers, originate from a failure in describing the C−F bond dissociation. To this end, we have first computed an ab initio benchmark for the C−F bond strength, that is, the dissociation energy D_{CF} associated with the reaction $H_3C{-}F \rightarrow CH_3^{\bullet} + F^{\bullet}$ at the same levels of theory as we did for the PES of the oxidative addition of the fluoromethane C−F bond to Pd. This was done again using the BLYP-optimized geometries, which yield a C−H bond length of 1.084 Å for the $D3_h$ symmetric methyl radical. Thus, we arrive at a dissociation energy of 111.9 kcal/mol at CCSD(T) with basis set BS7 and with counterpoise correction (HF: 75.8, MP2: 118.3, and CCSD: 108.5 kcal/mol; for details, see Table S3 in the Supporting Information), in nice agreement with the experimental value for the enthalpy at 0 K, namely 113.3 ± 3.8 kcal/mol.[90] Most functionals are able to describe the dissociation energy reasonably well, yielding errors, compared

TABLE 9: Energies (in kcal/mol) Relative to the Reactant Complex (RC) of Selected Stationary Points of Interest[a] along the Reaction Coordinates of the Two Pathways for Oxidative Addition of Pd to the C−F Bond of CH_3F, Computed for 26 Different Density Functionals with the ae-TZ2P Basis Set with All Electrons Treated Variationally[b]

method	R	TS_{OxIn}	$TS_{S_N2\text{-}ra}$	P	mean abs. err. rel. to RC[c]	err. in OxIn barr. rel. to RC[c]	err. in S_N2-ra barr. rel. to RC[c]
				LDA			
VWN	21.4	23.8	38.0	−8.0	9.3	−9.3	−4.8
				GGAs			
BP86	9.0	23.6	36.5	−9.6	7.0	−9.5	−6.3
BLYP	5.5	23.2	35.5	−10.8	6.8	−9.9	−7.3
Becke88x + BR89c	6.1	23.4	35.7	−12.6	7.3	−9.7	−7.1
PW91	10.5	23.7	36.6	−9.2	7.2	−9.4	−6.2
PBE	10.0	23.7	36.5	−9.0	7.1	−9.4	−6.3
FT97	10.8	26.4	37.4	−6.8	5.8	−6.7	−5.3
revPBE	5.0	24.0	36.1	−9.3	6.1	−9.1	−6.7
HCTH/93	−0.1	26.5	39.3	−5.3	4.9	−6.6	−3.5
RPBE	4.5	23.9	36.0	−9.3	6.3	−9.2	−6.8
BOP	2.1	23.7	35.4	−10.9	7.5	−9.4	−7.3
HCTH/120	4.2	25.8	39.3	−5.4	4.1	−7.3	−3.5
HCTH/147	3.5	25.8	39.3	−5.6	4.3	−7.3	−3.5
HCTH/407	1.6	27.2	40.4	−3.6	3.6	−5.9	−2.4
OLYP	−0.3	25.6	38.1	−6.6	5.8	−7.5	−4.7
				Meta-GGAs			
BLAP3	−0.4	26.3	37.4	−10.5	6.8	−6.8	−5.4
VS98	9.3	21.5	38.2	−9.3	7.1	−11.6	−4.6
KCIS	7.0	22.0	36.0	−11.4	7.5	−11.1	−6.8
PKZB	5.5	21.9	36.4	−12.3	7.3	−11.2	−6.4
Bmτ1	−0.7	26.1	37.2	−10.7	7.1	−7.0	−5.6
OLAP3	−6.2	28.7	40.0	−6.3	6.0	−4.4	−2.8
TPSS	7.0	22.9	38.5	−11.6	6.7	−10.2	−4.3
				Hybrid Functionals			
B3LYP	3.4	30.2	43.5	−3.6	2.0	−2.9	0.7
O3LYP	−0.3	30.8	44.9	−0.6	2.6	−2.3	2.1
X3LYP	3.9	30.8	44.2	−2.9	1.8	−2.3	1.4
TPSSh	5.7	26.5	42.1	−7.9	3.6	−6.6	−0.7

[a] Geometries optimized at ZORA-BLYP/TZ2P with frozen-core approximation, see Figure 1. [b] Computed post-SCF using the BLYP electron density. Relativistic effects treated with ZORA (see section 2.1). [c] Mean absolute error for the relative energies of the four stationary points RC, TS_{OxIn}, $TS_{S_N2\text{-}ra}$, and P relative to the reactant complex (RC) and error in the central barriers, i.e., in the energy of the TS_{OxIn}, respectively $TS_{S_N2\text{-}ra}$, relative to RC, compared with the CCSD(T) benchmark from this work.

with the CCSD(T) benchmark, in the order of a few kcal/mol. For BLYP the dissociation energy D_{CF} is overestimated by only 2.7 kcal/mol, while for B3LYP it is underestimated by a mere 1.0 kcal/mol (see Table 8). This agrees well with computations of the C−F bond strength by Wiener and Politzer,[91] who find that the B3LYP value is 4 kcal/mol less bonding than the BLYP one. In conclusion, the underestimation of the activation energy by BLYP cannot be ascribed to a failure in describing the bond dissociation (in fact, the slight error in the latter should raise the value of the barrier). Rather, it may be related to the overbinding between Pd and the methyl and fluoride ligands in later stages of the reaction (compare relative energies for P in Table 6).

3.5. BLYP//LDA: A Reasonable Compromise between Accuracy and Economy. The above shows that BLYP is a sound and more efficient alternative to highly correlated but computationally immensely demanding ab initio methods for the routine investigation of catalytic bond activation, also in larger, more realistic model systems. But one can, of course, always raise the size of a model system and thus the computational costs beyond the limits associated with the available computing resources. The question is as follows: can we push these limits even a bit further, that is, can we find a DFT approach that is not much less accurate than BLYP and yet significantly more efficient. The latter, i.e., a substantial improvement of the efficiency is easily achieved with LDA. However, it is well-known and also confirmed in this study (see Table 6) that LDA fails miserably regarding the quantitative accuracy of its PES. On the other hand, we have also seen that although LDA (VWN) geometries of stationary points differ somewhat more from the GGA ones than the latter differ among each other, this LDA versus GGA discrepancy in geometries is not dramatic (see Table 2). Therefore, in an attempt to achieve the utmost in terms of efficiency without losing too much accuracy, we have also computed the BLYP//LDA potential energy surfaces associated with the reactions of Pd + CH_3F, i.e., using LDA-optimized geometries of the stationary points at which then, in a single-point fashion, BLYP energies are computed (in all cases, again, using ZORA for relativistic effects and the TZ2P basis with frozen-core approximation). The energies relative to reactants are −2.0 kcal/mol for the reactant complex (RC), 19.7 kcal/mol for the activation barrier of the oxidative insertion pathway (TS_{OxIn}), 31.2 kcal/mol for the activation barrier of the alternative S_N2-ra pathway ($TS_{S_N2\text{-}ra}$), and −14.3 kcal/mol for the product (P) (values not shown in a Table). This compares reasonably well with the values obtained with a full BLYP//BLYP approach, i.e., using BLYP-optimized geometries (see Table 6). The BLYP//LDA relative energies are somewhat higher than those obtained with BLYP//BLYP, namely, 3.5, 2.1, 1.0, and 1.5 kcal/mol, respectively, for the four stationary points RC, TS_{OxIn}, $TS_{S_N2\text{-}ra}$, and P. Thus, the more approximate BLYP//LDA potential energy surface agrees even somewhat better with the CCSD(T) benchmark than BLYP//BLYP. While this is most probably fortuitous, it shows that the more approximate BLYP//LDA approach differs in this case only a few kcal/mol from the principally more accurate BLYP//

BLYP approach, while an enormous reduction in computational cost in the most demanding part of the computations (i.e., the geometry optimization) is achieved.

4. Conclusions

We have computed an ab initio benchmark for the archetypal oxidative addition of the fluoromethane C−F bond to palladium that derives from a hierarchical series of relativistic ab initio methods and highly polarized basis sets for the palladium atom, up to the counterpoise corrected, four-component spin-free Dirac-Coulomb CCSD(T)/(24*s*16*p*13*d*+4*f*+*p*+*g*) level, which is converged with respect to the basis-set size within a few tenths of a kcal/mol. Our findings stress the importance of sufficient higher-angular momentum polarization functions, *f* and *g*, as well as counterpoise correction for obtaining reliable activation energies.

This benchmark is used to evaluate the performance of 26 relativistic (ZORA) density functionals for describing geometries and relative energies of stationary points on the potential energy surface. Excellent agreement with our ab initio benchmark for energies relative to reactants is achieved by functionals of the GGA and meta-GGA as well as hybrid DFT approaches, each of which have a representative in the top three, with mean absolute errors as small as 2.7 kcal/mol or less. The outstanding performance of BLYP as compared to other functionals (e.g., OLYP and B3LYP), found for insertion of Pd into C−H and C−C bonds,[22,23] is not found for insertion of Pd into the C−F bond. Here, BLYP has a mean absolute error of 6.9 kcal/mol, which has to be compared with 2.2 kcal/mol for OLYP and even 1.5 kcal/mol for B3LYP. In particular, BLYP underestimates the overall barrier for OxIn by −10.1 kcal/mol and the overall barrier for S_N2-ra by −7.4 kcal/mol. For comparison, OLYP and B3LYP only slightly underestimate the overall barrier for OxIn, by −1.8 and −0.9 kcal/mol, respectively, and they slightly overestimate the barrier for S_N2-ra, by 1.0 and 2.7 kcal/mol, respectively.

Importantly, however, all important features of the CCSD(T) benchmark potential energy surfaces are reproduced by important functionals such as BLYP, OLYP, and B3LYP. Thus, while none of these functionals is the "very best one" for each individual model reaction, they all agree with the CCSD(T) benchmark that, for example, the activation energies for oxidative addition are in the following order: C−F (via S_N2-ra) > C− F (OxIn) ≳ C−C (OxIn) > C−H (OxIn). Our DFT results have been verified to be converged with the basis-set size at ZORA-BLYP/TZ2P and to be unaffected by the frozen-core approximation for the core shells of carbon (1*s*), chlorine (1*s*2*s*2*p*), and palladium (1*s*2*s*2*p*3*s*3*p*3*d*). We consider this a sound and efficient approach for the routine investigation of catalytic bond activation, also in larger, more realistic model systems.

Acknowledgment. We thank the Nederlandse Organisatie voor Wetenschappelijk Onderzoek (NWO-CW and NWO-NCF) for financial support.

Supporting Information Available: Total energies of all stationary points involved at all levels of ab initio theory applied in the computations. This material is available free of charge via the Internet at http://pubs.acs.org.

References and Notes

(1) Smart, B. E. Fluorocarbons. In *The Chemistry of Functional Groups, Supplement D*; Patai, S., Rappoport, Z., Eds.; Wiley: New York, 1983; p 603.
(2) Kiplinger, J. L.; Richmond, Th. G.; Osterberg, C. E. *Chem. Rev.* **1994**, *94*, 373.
(3) Burdeniuc, J.; Jedlicka, B.; Crabtree, R. H. *Chem. Ber.* **1997**, *130*, 145.
(4) Böhm, V. P. W.; Gstöttmayr, C. W. K.; Weskamp, Th.; Herrmann, W. A. *Angew. Chem., Int. Ed.* **2001**, *40*, 3387.
(5) Senn, H. M.; Ziegler, T. *Organometallics* **2004**, *23*, 2980.
(6) Bickelhaupt, F. M.; Ziegler, T.; Ragué Schleyer, P. v. *Organometallics* **1995**, *14*, 2288.
(7) Albert, K.; Gisdakis, Ph.; Rösch, N. *Organometallics* **1998**, *17*, 1608.
(8) Sundermann, A.; Uzan, O.; Martin, J. M. L. *Chem. Eur. J.* **2001**, *7*, 1703.
(9) Diefenbach, A.; Bickelhaupt, F. M. *J. Chem. Phys.* **2001**, *115*, 4030.
(10) Smurnyi, E. D.; Gloriozov, I. P.; Ustynuk, Yu. A. *Russ. J. Phys. Chem.* **2003**, *77*, 1699.
(11) Reinhold: M.; McGrady, J. E.; Perutz, R. N. *J. Am. Chem. Soc.* **2004**, *126*, 5268.
(12) Diefenbach, A.; Bickelhaupt, F. M. *J. Phys. Chem. A* **2004**, *108*, 8460.
(13) Diefenbach, A.; de Jong, G. Th.; Bickelhaupt, F. M. *J. Chem. Theory Comput.* **2005**, *1*, 286.
(14) Diefenbach, A.; de Jong, G. Th.; Bickelhaupt, F. M. *Mol. Phys.* **2005**, *103*, 995.
(15) Dedieu, A. *Chem. Rev.* **2000**, *100*, 543.
(16) Møller, C.; Plesset, M. S. *Phys. Rev.* **1934**, *46*, 618.
(17) Cizek, J. *J. Chem. Phys.* **1966**, *45*, 4256.
(18) Purvis III, G. D.; Bartlett, R. J. *J. Chem. Phys.* **1982**, *76*, 1910.
(19) Raghavachari, K.; Trucks, G. W.; Pople, J. A.; Head-Gordon, M. *Chem. Phys. Lett.* **1989**, *157*, 479.
(20) Boys, S. F.; Bernardi, F. *Mol. Phys.* **1970**, *19*, 553.
(21) de Jong, G. Th.; Solà, M.; Visscher, L.; Bickelhaupt, F. M. *J. Chem. Phys.* **2004**, *121*, 9982.
(22) de Jong, G. Th.; Geerke, D. P.; Diefenbach, A.; Bickelhaupt, F. M. *Chem. Phys.* **2005**, *313*, 261.
(23) de Jong, G. Th.; Geerke, D. P.; Diefenbach, A.; Solà, M.; Bickelhaupt, F. M. *J. Comput. Chem.* **2005**, *26*, 1006.
(24) Hohenberg, P.; Kohn, W. *Phys. Rev.* **1964**, *136*, B864.
(25) Kohn, W.; Sham, L. J. *Phys. Rev.* **1965**, *140*, A1133.
(26) Parr, R. G.; Yang, W. *Density-Functional Theory of Atoms and Molecules*; Oxford University Press: New York, 1989.
(27) Baker, J.; Muir, M.; Andzelm, J. *J. Chem. Phys.* **1995**, *102*, 2063.
(28) Barone, V.; Adamo, C. *J. Chem. Phys.* **1996**, *105*, 11007.
(29) Thümmel, H. T.; Bauschlicher, C. W., Jr. *J. Phys. Chem. A* **1997**, *101*, 1188.
(30) Bach, R. D.; Glukhovtsev, M. N.; Gonzales, C. *J. Am. Chem. Soc.* **1998**, *120*, 9902.
(31) Gritsenko, O. V.; Ensing, B.; Schippers, P. R. T.; Baerends, E. J. *J. Phys. Chem. A* **2000**, *104*, 8558.
(32) Poater, J.; Solà, M.; Duran, M.; Robles, J. *Phys. Chem. Chem. Phys.* **2002**, *4*, 722.
(33) Nibbering, N. M. M. *Adv. Phys. Org. Chem.* **1988**, *24*, 1.
(34) Carroll, J. J.; Weisshaar, J. C. *J. Am. Chem. Soc.* **1993**, *115*, 800.
(35) Bickelhaupt, F. M. *Mass Spectrom. Rev.* **2001**, *20*, 347.
(36) Baerends, E. J.; Ellis, D. E.; Ros, P. *Chem. Phys.* **1973**, *2*, 41.
(37) Fonseca Guerra, C.; Snijders, J. G.; te Velde, G.; Baerends, E. J. *Theor. Chem. Acc.* **1998**, *99*, 391.
(38) te Velde, G.; Bickelhaupt, F. M.; Baerends, E. J.; Fonseca Guerra, C.; van Gisbergen, S. J. A.; Snijders, J. G.; Ziegler, T. *J. Comput. Chem.* **2001**, *22*, 931.
(39) Baerends, E. J.; et al. Computer code ADF2002.03; SCM, Theoretical Chemistry, Vrije Universiteit: Amsterdam, The Netherlands, 2002.
(40) Vosko, S. H.; Wilk, L.; Nusair, M. *Can. J. Phys.* **1980**, *58*, 1200.
(41) Becke, A. D. *Phys. Rev. A* **1988**, *38*, 3098.
(42) Perdew, J. P. *Phys. Rev. B* **1986**, *33*, 8822.
(43) Lee, C.; Yang, W.; Parr, R. G. *Phys. Rev. B* **1988**, *37*, 785.
(44) Perdew, J. P. In *Electronic structure of solids '91*; Ziesche, P., Eschrig, H., Eds.; Akademie Verlag: Berlin, 1991.
(45) Perdew, J. P.; Wang, Y. *Phys. Rev. B* **1992**, *45*, 13244.
(46) Perdew, J. P.; Chevary, J. A.; Vosko, S. H.; Jackson, K. A.; Pederson, M. R.; Singh, D. J.; Fiolhais, C. *Phys. Rev. B* **1992**, *46*, 6671.
(47) Perdew, J. P.; Chevary, J. A.; Vosko, S. H.; Jackson, K. A.; Pederson, M. R.; Singh, D. J.; Fiolhais, C. *Phys. Rev. B* **1993**, *49*, 4978(E).
(48) Perdew, J. P.; Burke, K.; Ernzerhof, M. *Phys. Rev. Lett.* **1996**, *77*, 3865.
(49) Perdew, J. P.; Burke, K.; Ernzerhof, M. *Phys. Rev. Lett.* **1997**, *78*, 1396(E).
(50) Zhang, Y.; Yang, W. *Phys. Rev. Lett.* **1998**, *80*, 890.
(51) Hammer, B.; Hansen, L. B.; Nørkov, J. K. *Phys. Rev. B* **1999**, *59*, 7413.
(52) Handy, N. C.; Cohen, A. J. *Mol. Phys.* **2001**, *99*, 403.
(53) van Lenthe, E.; Baerends, E. J.; Snijders, J. G. *J. Chem. Phys.* **1994**, *101*, 9783.

(54) Visscher, L.; Lee, T. J.; Dyall, K. G. *J. Chem. Phys.* **1996**, *105*, 8769.
(55) Jensen, H. J. Aa.; Saue, T.; Visscher, L. Computer code DIRAC, release 4.0; Syddansk Universitet: Odense, Denmark, 2004.
(56) Dyall, K. G. *J. Chem. Phys.* **1994**, *100*, 2118.
(57) Visscher, L. *Theor. Chem. Acc.* **1997**, *98*, 68.
(58) Dunning, Th. H., Jr. *J. Chem. Phys.* **1989**, *90*, 1007.
(59) Kendall, R. A.; Dunning, Th. H., Jr.; Harrison, R. J. *J. Chem. Phys.* **1992**, *96*, 6796.
(60) Visscher, L.; Aerts, P. J. C.; Visser, O.; Nieuwpoort, W. C. *Int. J. Quantum Chem.: Quantum Chem. Symp.* **1991**, *25*, 131.
(61) Ehlers, A. W.; Böhme, M.; Dapprich, S.; Gobbi, A.; Höllwarth, A.; Jonas, V.; Köhler, K. F.; Stegmann, R.; Veldkamp, A.; Frenking, G. *Chem. Phys. Lett.* **1993**, *208*, 111.
(62) Langhoff, S. R.; Petterson, L. G. M.; Bauschlicher, C. W., Jr. *J. Chem. Phys.* **1987**, *86*, 268.
(63) Osanai, Y.; Sekiya, M.; Noro, T.; Koga, T. *Mol. Phys.* **2003**, *101*, 65.
(64) Becke, A. D. *J. Chem. Phys.* **1988**, *88*, 1053.
(65) Becke, A. D.; Roussel, M. R. *Phys. Rev. A* **1989**, *39*, 3761.
(66) Filatov, M.; Thiel, W. *Mol. Phys.* **1997**, *91*, 847.
(67) Hamprecht, F. A.; Cohen, A. J.; Tozer, D. J.; Handy, N. C. *J. Chem. Phys.* **1998**, *109*, 6264.
(68) Tsuneda, T.; Suzumura, T.; Hirao, K. *J. Chem. Phys.* **1999**, *110*, 10664.
(69) Boese, A. D.; Doltsinis, N. L.; Handy, N. C.; Sprik, M. *J. Chem. Phys.* **2000**, *112*, 1670.
(70) Boese, A. D.; Handy, N. C. *J. Chem. Phys.* **2001**, *114*, 5497.
(71) Proynov, E. I.; Sirois, S.; Salahub, D. R. *Int. J. Quantum Chem.* **1997**, *64*, 427.
(72) van Voorhis, T.; Scuseria, G. E. *J. Chem. Phys.* **1998**, *109*, 400.
(73) Krieger, J. B.; Chen, J.; Iafrate, G. J.; Savin, A. In *Electron correlation and material properties*; Gonis, A., Kioussis, N., Eds.; Plenum: New York, 1999.
(74) Perdew, J. P.; Kurth, S.; Zupan, A.; Blaha, P. *Phys. Rev. Lett.* **1999**, *82*, 2544.
(75) Perdew, J. P.; Kurth, S.; Zupan, A.; Blaha, P. *Phys. Rev. Lett.* **1999**, *82*, 5179(E).
(76) Proynov, E.; Chermette, H.; Salahub, D. R. *J. Chem. Phys.* **2000**, *113*, 10013.
(77) Tao, J.; Perdew, J. P.; Staroverov, V. N.; Scuseria, G. E. *Phys. Rev. Lett.* **2003**, *91*, 146401.
(78) Staroverov, V. N.; Scuseria, G. E.; Tao, J.; Perdew, J. P. *J. Chem. Phys.* **2003**, *119*, 12129.
(79) Becke, A. D. *J. Chem. Phys.* **1993**, *98*, 5648.
(80) Stephens, P. J.; Devlin, F. J.; Chabalowski, C. F.; Frisch, M. J. *J. Phys. Chem.* **1994**, *98*, 11623.
(81) Cohen, A. J.; Handy, N. C. *Mol. Phys.* **2001**, *99*, 607.
(82) Xu, X.; Goddard, W. A., III *Proc. Natl. Acad. Sci. U.S.A.* **2004**, *101*, 2673.
(83) Hertwig, R. H.; Koch, W. *Chem. Phys. Lett.* **1997**, *268*, 345.
(84) Frenking, G.; Antes, I.; Böhme, M.; Dapprich, S.; Ehlers, A. W.; Jonas, V.; Neuhaus, A.; Otto, M.; Stegmann, R.; Veldkamp, A.; Vyboishchikov, S. F. Pseudopotential calculations of transition metal compounds. In *Reviews in Computational Chemistry*; Lipkowitz, K. B., Boyd, D. B., Eds.; VCH Publishers Inc.: New York, 1996; Vol. 8, p 63.
(85) Cundari, Th. R.; Benson, M. T.; Lutz, M. L. Effective core potential approaches to the chemistry of heavier elements. In *Reviews in Computational Chemistry*; Lipkowitz, K. B., Boyd, D. B., Eds.; VCH Publishers Inc.: New York, 1996; Vol. 8, p 145.
(86) Hay, P. J.; Wadt, W. R. *J. Chem. Phys.* **1985**, *82*, 299.
(87) Jonas, V.; Frenking, G.; Reetz, M. T. *J. Comput. Chem.* **1992**, *13*, 919.
(88) Bickelhaupt, F. M.; Baerends, E. J.; Nibbering, N. M. M. *Chem. Eur. J.* **1996**, *2*, 196.
(89) Bickelhaupt, F. M. *J. Comput. Chem.* **1999**, *20*, 114.
(90) NIST Computational Chemistry Comparison and Benchmark Database, NIST Standard Reference Database Number 101, Release 11, May 2005, R. D. Johnson III, Ed.; http://srdata.nist.gov/cccbdb.
(91) Wiener, J. J.; Politzer, P. *J. Mol. Struct. (THEOCHEM)* **1998**, *427*, 171.